Received: 17 February 2019 | Revised: 28 February 2019 | Accepted: 28 February 2019

DOI: 10.1002/er.4505

REVIEW PAPER

WILEY INTERNATIONAL JOURNAL OF ENERGY RESEARCH

A review of synthesis and morphology of $SrTiO_3$ for energy and other applications

Bao Lee Phoon[1] | Chin Wei Lai[1] | Joon Ching Juan[1,2] | Pau-Loke Show[3] | Wei-Hsin Chen[4,5]

[1]Nanotechnology & Catalysis Research Centre (NANOCAT), Level 3 Block A, IPS Building, Institute for Advanced Studies, University of Malaya, Kuala Lumpur, Malaysia

[2]School of Science, Monash University, Sunway Campus, Jalan Lagoon Selatan, Malaysia

[3]Department of Chemical and Environmental Engineering, Faculty of Engineering, University of Nottingham Malaysia Campus, Semenyih, Malaysia

[4]Department of Aeronautics and Astronautics, National Cheng Kung University, Tainan, Taiwan

[5]Research Center for Energy Technology and Strategy, National Cheng Kung University, Tainan, Taiwan

Correspondence

Joon Ching Juan, Nanotechnology & Catalysis Research Centre (NANOCAT), Level 3 Block A, IPS Building, Institute for Advanced Studies, University of Malaya, 50603 Kuala Lumpur, Malaysia.
Email: jcjuan@um.edu.my

Pau-Loke Show, Department of Chemical and Environmental Engineering, Faculty of Engineering, University of Nottingham Malaysia Campus, Jalan Broga, 43500 Semenyih, Selangor Darul Ehsan, Malaysia.
Email: pauloke.show@nottingham.edu.my, showpauloke@gmail.com

Wei-Hsin Chen, Department of Aeronautics and Astronautics, National Cheng Kung University, Tainan 701, Taiwan.
Email: weihsinchen@gmail.com, chenwh@mail.ncku.edu.tw

Funding information

University of Malaya, Grant/Award Number: ST010-2017; Ministry of Education Malaysia, Grant/Award Number: PR002-2016A

Summary

With the increasing demand and depleting trend of commercial energies, it has forced the researchers all over the world to accelerate research and development in the area of renewable energy. Currently, unique and interesting features of binary compounds have gained more attention by researchers, and it became a favourite research topic among various groups of researchers around this world. It was noticed that strontium titanate ($SrTiO_3$) consists of several extraordinary properties that can apply for miscellaneous applications especially for energy storage, fuel cells, as well as to generate hydrogen fuel via photocatalysis process. Besides that, it was noticed that $SrTiO_3$ can be synthesised in different pathways. The method of preparation and amount of precursors can affect the surface properties of $SrTiO_3$. Thus, this article presents a critical review on how $SrTiO_3$ synthesis methods affect its surface morphology and the applications of $SrTiO_3$ in various fields.

KEYWORDS

ceramics, energy storage, hydrogen production, nanomaterials, nanoparticles, perovskite, $SrTiO_3$

1 | INTRODUCTION

Perovskite is a material class that consists of ternary oxides of a structure ABO_3, where A is mostly a group I or II element whereas B is mostly a transition metal. This perovskite-like structure was named in 1839 after the discovery of $CaTiO_3$ perovskite mineral. The occupation of the A and B sites is very variable, since the atomic radii of cations from periodic table can be varied because of different valence states. As a result, the real perovskite structure may show some lattice distortion in varying degrees compared with the ideal cubic perovskite ABO_3, thereby resulting crystal phases transformation phenomenon.

Strontium titanate, $SrTiO_3$, is a perovskite structure material (Figure 1), the cubic unit cell of $SrTiO_3$ with a lattice parameter of 3.905 Å. The octahedral corner–shared TiO_6 unit forms a tightly bonded network, which makes up the structural backbone of the lattice.[1,2] The melting point of $SrTiO_3$ is as high as 2080°C, making it applicable for high temperatures applications. $SrTiO_3$ exhibited as cubic perovskite structure at ambient temperature and pressure. If $SrTiO_3$ structure was cooled down to 105 K or lower, phase transition can occur from a cubic structure (space group: Pm3m) to a tetragonal (space group: P4mm). This phase transition was together with the changes of electrical properties. Normally, such a phase transition would give rise to ferroelectricity. However, up to 0 K, the $SrTiO_3$ does not display such transition. For this reason, the $SrTiO_3$ belongs to a class of quantum paraelectric or incipient ferroelectrics.

$SrTiO_3$ is a material with a wide range of unique properties. $SrTiO_3$ often applied as a substrate for the epitaxial growth of high temperature superconductors. Besides that, $SrTiO_3$ can be used in macroelectronics, ferroelectric, and optoelectronics applications. $SrTiO_3$ has a dielectric constant with high value (approximately 300) at ambient temperature and much larger at lower temperatures (approximately 10^4).[3] $SrTiO_3$ undergoes a metal insulator transition upon light doping. $SrTiO_3$ is a typical nonpolar band insulator with the band gap of 3.2 eV (indirect). However, with a flexible tunability in electrical conductivity, it can exhibit as metallic phase depending on the oxygen concentration.[4]

The bare $SrTiO_3$ is an electronic insulator at room temperature. Incorporation of point defects into the lattice can generate free charge carriers or charged ionic species. In semiconducting $SrTiO_3$ at room temperature, the charge carriers are predominately electrons introduced by donor impurity doping or heating in a reducing atmosphere. The latter treatment introduces an approximately equivalent density of oxygen vacancies, which are known to exhibit significantly large lattice mobility, particularly at elevated temperatures. Therefore, $SrTiO_3$ is considered as a mixed electronic-ionic conductor.

$SrTiO_3$ is a promising photocatalyst especially for the water splitting process. By comparing with TiO_2 band gap, $SrTiO_3$ band edge for the conduction band (CB) is about 200 mV more negative. Most importantly, $SrTiO_3$ has a high stability for thermal and chemical. Besides that, it was reported that the Sr^{2+} from the structure is able to accept electrons in the CB of photocatalyst to form Sr^{+}.[5] Then the as-formed Sr^{+} may also transport an electron to produce $O_2^{\cdot -}$ for organic compound decomposition, which restrains the photogenerated charge carriers recombination. Hence, $SrTiO_3$ was gained attention by many researchers in this recent year due to its

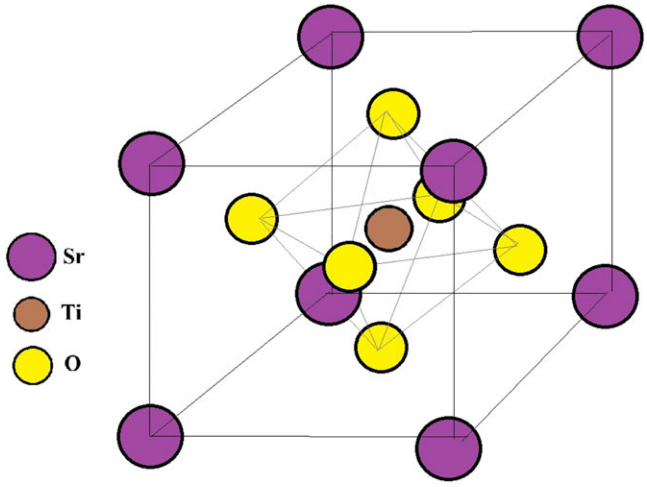

FIGURE 1 The lattice structure of $SrTiO_3$ [Colour figure can be viewed at wileyonlinelibrary.com]

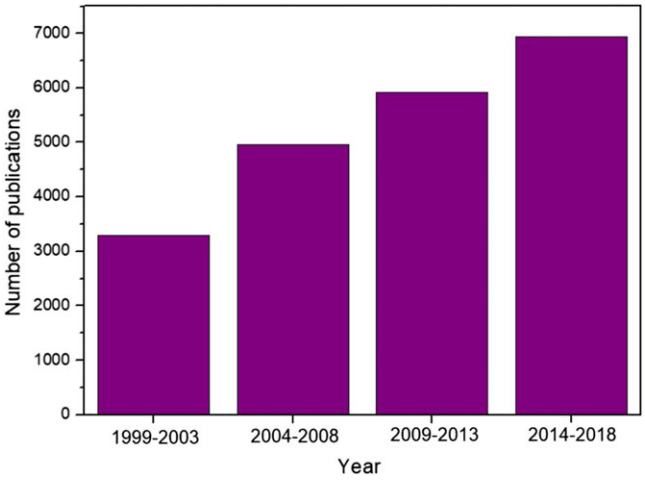

FIGURE 2 Number of publications using "strontium titanate" or "$SrTiO_3$" as the topic keywords in the past 20 years. Adapted from ISI Web of Science (WoS), dated 27 January 2019 [Colour figure can be viewed at wileyonlinelibrary.com]

photocatalytic properties.[6] However, the band gap of pure $SrTiO_3$ was found to be 3.2 eV (indirect); in other words, $SrTiO_3$ is only photocatalytic active under UV region ($\lambda < 387.5$ nm).

On the basis of Figure 2, the amount of literature reports on $SrTiO_3$ materials has accelerated over the past 20 years, and nearly 7000 papers have been published successfully in between the years 2014 and 2018 for various applications. This indicates the importance and attraction of this demanding research. With the fast-increasing number of publications in $SrTiO_3$ materials, there is a lack of comprehensive review on $SrTiO_3$. It was reported that the $SrTiO_3$ can be produced in many techniques such as hydrothermal, solid-state reaction (SSR), and ultrasound assisted but the different synthesise pathway would lead to different morphology, crystallinity, uniformity, shape, and size of the $SrTiO_3$ nanoparticles.[7] Recent studies on $SrTiO_3$ have demonstrated it has high potential for practical use, such as fuel cells[8] and gas sensors.[9] However, the synthesis techniques and applications of $SrTiO_3$ are not comprehensively discussed. In this review, the effects of $SrTiO_3$ synthesis technique and the $SrTiO_3$ applications are critically discussed.

2 | SYNTHESIS METHOD OF $SrTiO_3$

There are various kinds of starting materials that can be used to prepare $SrTiO_3$ in different synthesis conditions. Basically, the heterogeneous catalysts activity is affected

TABLE 1 Recent publications (2008-2018) of the preparation methods of $SrTiO_3$ nano-materials

Preparation Method	Structure	Particle Size, nm	Reference (Year)
Sol-precipitation coupled with hydrothermal synthesis	Nanocubes	60-120	[13] (2008)
Polymerised complex	Nanoparticles	25-100	[10] (2008)
Solid-state reaction	Nanoparticles	110-150	[10] (2008)
Ball milling–assisted solid-state reaction	Nanoparticles	30	[10] (2008)
Sol-gel combustion	Nanopowders (spherical)	20-30	[14] (2008)
Sol-gel	Nanopowders	N/A	[15] (2009)
Molten salt reaction	Submicron crystallites and nanocrystals	20-184	[16] (2010)
Microwave heating technique	Nanopowders	28-68	[17] (2010)
Solvothermal	Nanoparticles	50-80	[18] (2010)
Molten salt reaction	Nanocubes	64-182	[19] (2011)
Microwave-assisted hydrothermal	Nanospheres	N/A	[20] (2012)
Microwave-assisted hydrothermal	Nanocubes	46-57	[12] (2012)
Sol-gel hydrothermal	Nanoparticles	30-150	[21] (2012)
Hydrothermal	Mesocrystals	100-200	[22] (2012)
Solvothermal	Nanocubes	Approximately 20	[23] (2013)
Sol-gel combustion	Nanoparticles	45-56	[24] (2013)
Hydrothermal	Nanocubes	20-200	[7] (2014)
Solvothermal	Nanocubes, nanospheres, nanoflakes	24-43	[25] (2014)
Rapid sol-precipitation	Nanocubes	4-13	[26] (2014)
Hydrothermal	Microspheres	30-46	[27] (2015)
Solid-state reaction (flux based)	Nanocubes	300	[28] (2015)
Electrospinning	Nanotubes	Approximately 100	[29] (2015)
Ultrasound-assisted wet chemical	Nanocrystals	7-17	[30] (2015)
Solid-state crystal growth (SSGC)	Single crystals	N/A	[31] (2016)
Flux-mediated method	Nanocubes (irregular shape)	200-3000	[32] (2016)
Hydrothermal	Core-shell microspheres	Approximately 700	[33] (2017)
Ultrasound-assisted hydrothermal	Mesoporous nanopowder	8-18	[34] (2017)
Hydrothermal	Nanocubes	30-56	[6] (2018)

Abbreviation: N/A, not available.

by crystallinity, surface area, size, and crystal phase. The photoexcited electrons reach the surface with short diffusion distance, and large surface area could be the advantages of nano-particulate photocatalysts. In this aspect, the precise control of the shape and size of $SrTiO_3$ is significant for developing high-performance photocatalyst and evaluating the shape-dependent photoreactivity. Besides that, the outer surface and morphology of photocatalyst also influence their activity of photocatalysis. In addition, it was noticed that the E_g values if $SrTiO_3$ could be slightly different when sample preparation method and different processing details was used. The $SrTiO_3$ nanoparticles band gap was determined to be nearly 3.10 eV by conventional SSR[10] and hydrothermal synthesis.[7] Also, it was reported by a researcher that $SrTiO_3$ nanoparticle was synthesised by SSR with ball milling assisted and the band gap is about 2.00 eV, which is photoactive in under irradiation of visible light.[10] It was noticed that metal impurities is in the $SrTiO_3$ lattice structure and this impurity was suspected to affect the E_g value of the sample.[10] The $SrTiO_3$ nanoparticle was estimated to be 3.35 eV when coprecipitation synthesis was used,[11] and about some researchers was synthesised $SrTiO_3$ nanoparticles with E_g value of 3.40 to 3.60 eV.[12] A lot of scientists have reported to produce $SrTiO_3$ in variety of methods (Table 1). It was found that hydrothermal reaction, solvothermal reaction, SSR, sonochemical, and sol-gel are the common methods for synthesising $SrTiO_3$. Different synthesis pathways would lead to different morphology, crystallinity, uniformity, size, and shape of $SrTiO_3$ nanoparticles.[7]

2.1 | Hydrothermal reaction

In the ceramics industry, hydrothermal reaction is a widespread method for the small particles production nowadays. The reaction of hydrothermal is conducted in a vessel that designed with stainless steel (also known as autoclave) at a certain temperature and/or pressure with the reactions taking place in reaching the vapour saturation pressure. The amount of precursor added to the autoclave and the temperature ($420 < T < 750$ K) largely determines the pressure produced during the synthesising process ($100 < P < 300$ kbar). It was known that the hydrothermal reaction generally has better control of the shape and size distributions as well as the crystallinity compared with other synthesis techniques. It has been used to synthesise $SrTiO_3$ nanoparticles with or without the aid of surfactants. Moreover, photocatalyst calcination is unnecessary as the crystal $SrTiO_3$ is readily formed in the autoclave chamber.

Figure 3 shows the procedure of hydrothermal process. It was proposed that the hydrothermal reaction to synthesise $SrTiO_3$ is a dissolution-precipitation process.[7,35] Step (1) indicates that strontium precursor hydrolyses to

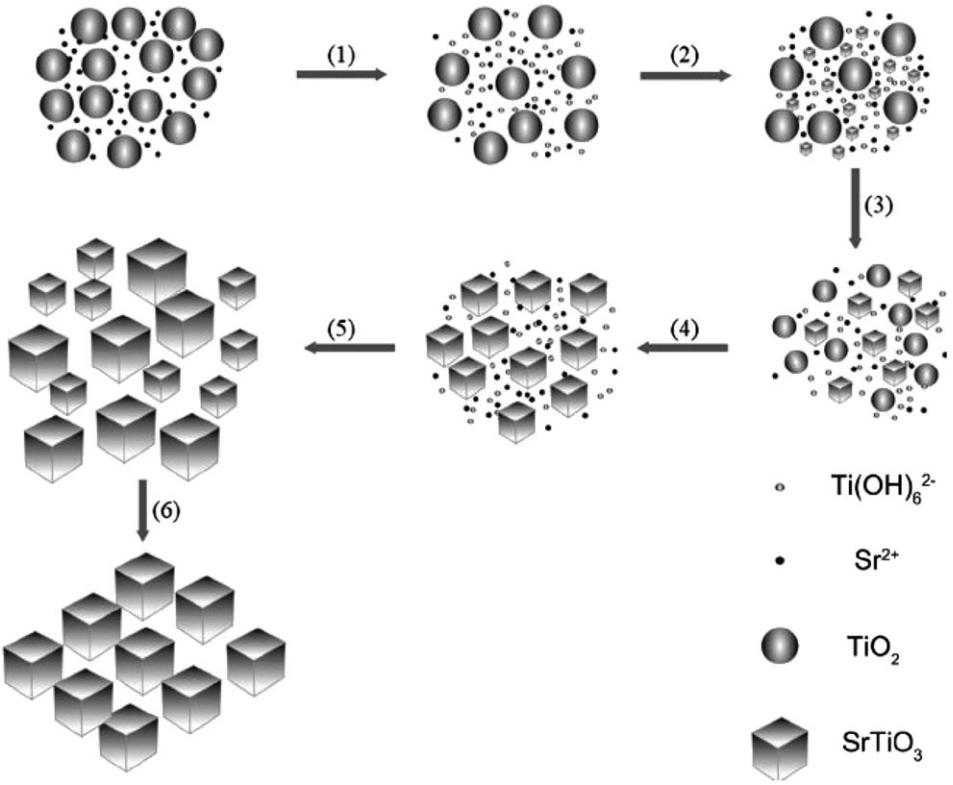

FIGURE 3 The hydrothermal reaction process to synthesise $SrTiO_3$. Reproduced and reprinted from Zhang et al[35]

produce strontium ions. Then, the formation of soluble $[Ti(OH)_6]^{2-}$ complexes is taken place by crystalline TiO_2 powder (anatase) as the starting material reacts with hydroxide ions. The strontium ion and $[Ti(OH)_6]^{2-}$ complexes were then integrate and precipitate mutually to produce a new $SrTiO_3$ phase. In step (4), as the reaction of dissolution-precipitation carry on, the TiO_2 starting material is dissolved slowly. Then, $SrTiO_3$ grains continue to emerge until the TiO_2 starting materials are totally consumed. Finally, after the reaction of dissolution-precipitation accomplishes, the small grains of $SrTiO_3$ were gradually grown up to become large grains and uniform size of nanoparticles is formed.

Some researchers were done the $SrTiO_3$ synthesis by different hydrothermal parameters as listed in Table 2. According to Table 2, different synthesis condition (eg, temperature, pH, and time) makes possible tuning the shapes of $SrTiO_3$ ranging from nanoparticles during hydrothermal reaction. It was reported that the alkaline medium is critically important role to dissolve the crystalline anatase TiO_2 powders to become a metal complex because the formation of soluble $[Ti(OH)_6]^{2-}$ complex requires that the bonding of Ti-O on the TiO_2 precursor must undergo hydrolytic attack in order to break the bond. After that, precipitation of $SrTiO_3$ can only take place.[7] A regular hydrothermal reaction would require the precursors mixing with the desired solvent as the medium and is treated in an autoclave at high temperatures. Besides that, hydrothermal synthesis can also synthesise metal-doped $SrTiO_3$ with a uniform nanoparticle size.[40,43]

In 2014, Huang et al[7] reported that raise in the temperature of synthesis has resulted in the increase of the $SrTiO_3$ particle size, this justified that the stronger agglomeration at higher temperature, and it was proposed that 130°C of hydrothermal temperature produced the best morphology of $SrTiO_3$. In 2016, Shen et al[53] tried to synthesise $SrTiO_3$ without using alkaline medium in different hydrothermal temperatures. It was reported by Shen et al,[53] higher temperature of hydrothermal synthesis can cause nanoparticles aggregation and irregular growing particle, resulting in a heterogeneous microstructure. On the basis of the stability thermodynamic calculations for the hydrothermal system of Sr-Ti,[54] high pH and mole ratio of Sr/Ti larger than 1 were required in order to produce a high purity of $SrTiO_3$ nanocrystals.[7] It was reported that the $SrTiO_3$ able to form successfully by 1 hour of synthesis time basically.[37] However, the $SrTiO_3$ particles size and shape were not in uniform.[36] Huang et al[7] also reported the synthesis time could affect the $SrTiO_3$ nanoparticles size that would relate to process of Ostwald ripening where it is depended by both thermodynamic and kinetic effects. The $SrTiO_3$ nanoparticle size would grow larger when the reaction time prolonged. This is because at the reaction early stage, nucleation occurs and formed smaller particles, but the crystal growth process would occur at the prolonged time. Moreover, Zhang et al[35] proposed that the Sr/Ti mole fraction could directly influence the specific surface area and particle size in nucleation and crystal growth process. The short synthesis period and high mole fraction of Sr/Ti were helpful to synthesis large specific surface area and small particles of $SrTiO_3$. Meanwhile, long reaction time and lower mole fraction of Sr/Ti were advantageous for large particles with small specific surface area. In 2015, Mourão et al[27] reported a hydrothermal reaction of synthesis $SrTiO_3$ nanoparticles by studying the mechanical stirring parameter. Mechanical stirring is a significant parameter for the hydrothermal process. During the hydrothermal reaction, the stirring process could increase the particle collision that would affect the properties of the final product. However, conventional hydrothermal synthesis produced a high roughness of $SrTiO_3$ nanoparticles and aggregation was found. It was found that $SrCO_3$ phase was eliminated when mechanical stirring was applied. Besides that, the $SrTiO_3$ nanoparticles sample that undergoes stirring during the hydrothermal reactions shows a better photocatalytic activity compared with the final product that without stirring.

Most of the time, a secondary phase, orthorhombic $SrCO_3$ peak was observed together with $SrTiO_3$ under X-ray diffractogram (XRD) (Figure 4), and many researchers have reported the similar phenomenon.[7,35,43] It can be explained that during the process of both pretreatment and posttreatment, carbon dioxide (CO_2) in the air would dissolve in mixture as CO_3^{2-} and go through reaction with Sr^{2+} that come from the precursor, that is, $Sr(OH)_2.8H_2O$ (Equations 1 and 2). Under alkaline medium, the stated reaction is favourable and thus causes the existence of $SrCO_3$ peak. In addition, $SrCO_3$ is a compound with low solubility ($K_{sp} = 9.3 \times 10^{-10}$), and thus, it can go through solid formation although the CO_2 is in low concentration.[55] In addition, KOH is a good absorbent of CO_2 from the air. Hydroxide ions is a strong Lewis base; hence, the $SrCO_3$ arises from the effect of the hydroxide ions.[5]

$$CO_2\,(g) + H_2O\,(l) \rightleftharpoons 2\,H^+ + CO_3^{2-}\,(aq), \quad (1)$$

$$CO_3^{2-}\,(aq) + Sr^{2+} \rightleftharpoons SrCO_3\,(s). \quad (2)$$

Sometimes, hydrothermal reaction is incorporated with microwave synthesis, which is known as microwave-assisted hydrothermal (MAH) reaction.

TABLE 2 Hydrothermal parameters that studied by other researchers

Parameters							
Sr Precursor	Ti Precursor	Sr:Ti Mole Ratio	Alkaline Medium/ Molarity, M	Time, h	Temperature, °C	Particle Shape/Size, nm	Reference (Year)
$SrCl_2.6H_2O$	$TiCl_4$	N/A	KOH/4	0-6.2	20-60	Nanoparticles	[36] (2004)
$SrOH_2.8H_2O$	TiO_2 (P25)	10:1	KOH/50	1-120	150	Nanoparticles/20-50	[37] (2010)
$SrCl_2.6H_2O$	$C_{12}H_{28}TiO_4$	1:1	KOH	0-2.6	140	Nanocubes/46-57	[12] (2012)
Sr $(Ac)_2$. H_2O	Ti $(SO_4)_2$	N/A	KOH/2	24	240	Nanocrystals/100-200	[38] (2013)
$SrOH_2.8H_2O$	TiO_2 (P25)	1:1	NaOH/1-5	24	130	Nanocubes/20-200	[7] (2014)
$SrOH_2.8H_2O$	TiO_2 (P25)	1:1	NaOH/3	12-96	130	Nanocubes/20-200	[7] (2014)
$SrOH_2.8H_2O$	TiO_2 (P25)	1:1	NaOH/3	72	100-180	Nanocubes/20-200	[7] (2014)
Sr $(Ac)_2$	Ti$[OCH(CH_3)_2]_4$	N/A	NH_4OH	12	120	Porous nanoparticles/450-800	[39] (2014)
Sr $(Ac)_2$	TiO_2	N/A	KOH/10	24	220	Nanocubes/90-150	[40] (2014)
$SrOH_2.8H_2O$	TiO_2	1:1	N/A	40	160	Nanoparticles	[41] (2014)
Sr $(NO_3)_2$	TiB_2	1:1	NaOH/3	24-72	200	Nanoparticles	[42] (2014)
$SrOH_2.8H_2O$	TiO_2	1:1 and 1:2	NaOH/50	20-60	220	Nanoparticles/32-45	[35] (2015)
$SrCl_2.2H_2O$	$TiOSO_4$. yH_2SO_4. yH_2O	1:1	KOH/6	0-8	140	Microspheres/30-46	[27] (2015)
$SrCl_2.2H_2O$	$TiOSO_4$. yH_2SO_4. yH_2O	1:1	KOH/6	1	140	Microspheres/30-46 (with/ without stirring parameter)	[27] (2015)
$SrOH_2.8H_2O$	TiO_2 (P25)	1:1	KOH/3.5 mmol	72	150	Nanocubes/50	[43] (2015)
$SrOH_2.8H_2O$	TiO_2 nanotube array films	N/A	N/A	0-6	150	Nanotubes	[44] (2017)
$SrOH_2$	TiO_2 nanotubes	N/A	N/A	1-3	180	Nanotubes	[45] (2017)
$SrOH_2.8H_2O$	TiO_2	N/A	N/A	12	180	Nanocubes/20-50	[46] (2017)
Sr $(NO_3)_2$	Ti $(OBu)_4$	N/A	NaOH	24	180	Nanoparticles	[47] (2017)
$SrCl_2.6H_2O$	Ti $(OBu)_4$	N/A	NaOH/1	6	180	Microspheres	[48] (2017)
$SrOH_2.8H_2O$	TiO_2	1:1	KOH/3	72	60-180	Nanocubes/30-56	[6] (2018)
$SrOH_2.8H_2O$	$[CH_3CH(O^-)CO_2NH_4]_2Ti(OH)_2$	N/A	NaOH/5	72-120	150	Nanoparticles/20-40	[49] (2018)
Sr $(Ac)_2$	Ti $(OBu)_4$	1:1	Glycerol	N/A	240	Nanocubes/20-200	[50] (2018)
$SrOH_2.8H_2O$	$(C_4H_9O)_4Ti$	N/A	NaOH/12	20	90	Nanowires	[51] (2018)
$Sr(OH)_2$	TiO_2	1:0.98	NaOH/5	1	180	Nanocubes/10-100	[52] (2019)

Abbreviations: N/A, not available; Ac, CH_3COO; Bu, C_4H_9.

MAH uses short reaction period and low temperature because the radiation has interaction with water.[56] The use of microwave radiation incorporate with hydrothermal method shows itself, certainly, as an outstanding combination for the synthesis of nanomaterials. The microwave heating has a few merits over conventional hydrothermal preparation such as (i) high rate of heating and thus increasing the rate of reaction, (ii) outstanding control of reaction parameters, (iii) selective heating, if the mixture of reaction contains compound of different properties of microwave absorption, (iv) high fields, (v) improved selectivity because of low reaction field, (vi)

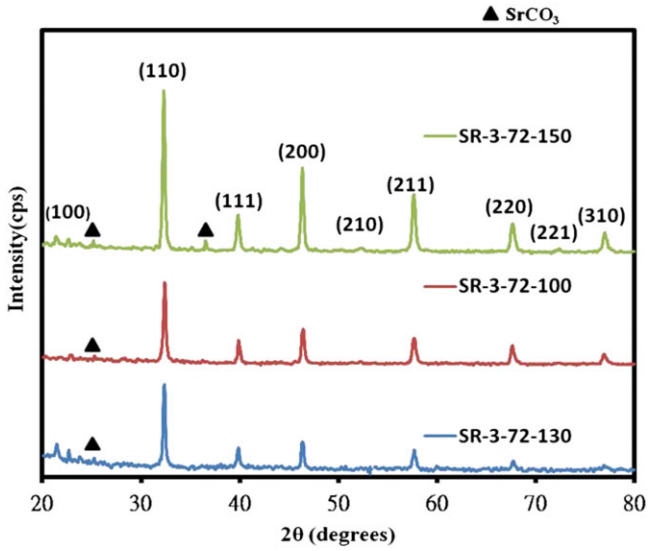

FIGURE 4 The X-ray diffractogram (XRD) of hydrothermal synthesised $SrTiO_3$ samples in different reaction temperatures. Reproduced from Huang et al[7] [Colour figure can be viewed at wileyonlinelibrary.com]

improved reproducibility, (vii) automation and high yield synthesis, and (viii) no direct contact between the reagent and heating source.[12,57,58] In 2012, Souza et al[12] synthesised $SrTiO_3$ using MAH; it was found that the $SrTiO_3$ particles formed successfully after 4 minutes of reaction. This was greatly reduced the reaction time as compared with conventional hydrothermal synthesis that required at least 1 hour for $SrTiO_3$ formation.[36,37] The microwave radiation with high frequency directly interacts with the mixture that consists of permanent water dipoles, initiating a rapid heating from rotation of molecule. Therefore, the radiation of microwave can promote a valid increase of ions collision rates, which favours the $SrTiO_3$ phase nucleation process. However, $SrTiO_3$ nanoparticles need to go through to process such as clusters formation, self-assembly, and finally crystal growth in order to produce uniform particles.

2.2 | Solvothermal reaction

Various solvents other than water can be employed for this solvothermal process; this technique is almost the same as the hydrothermal synthesis. The organic solvent such as carboxylic acids, ketones, toluene, and alcohols can be applied as the solvent medium.[59] Solvothermal synthesis has been determined to be a versatile route for the wide variety production of nanoparticles with uniform particle size, particularly when organic solvents with high boiling points are chosen. High crystalline final product using solvothermal synthesis was noticed because the organic solvents with low dielectric constant were used. This give rise to a decreased into solubility of samples, which restricts the process of dehydration and

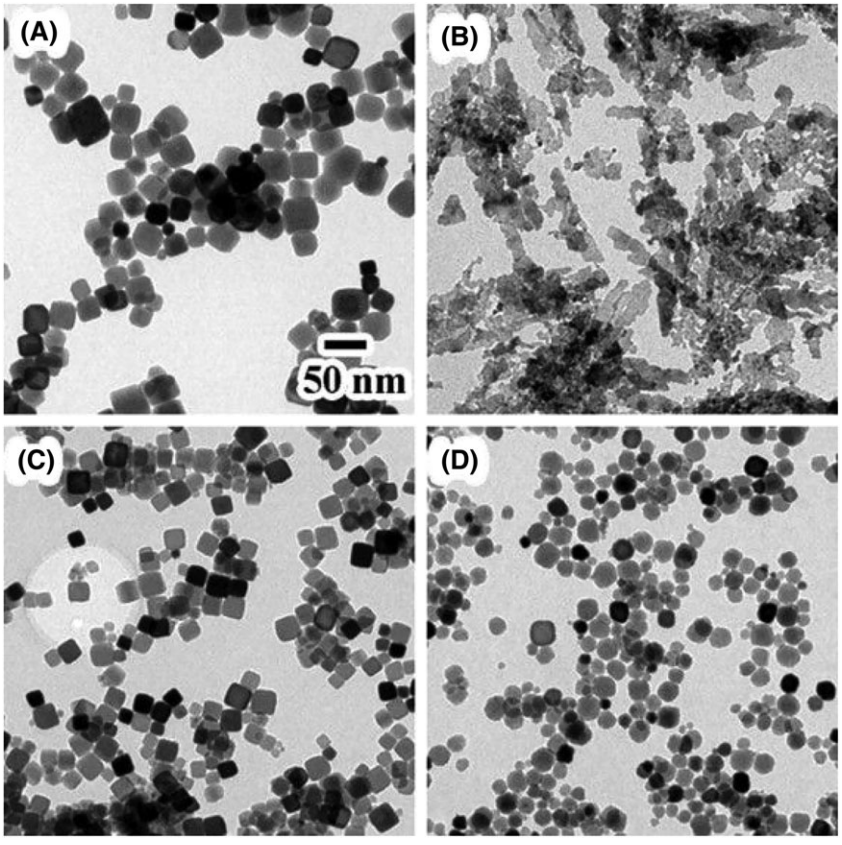

FIGURE 5 The scanning electron micrograph (SEM) of solvothermal synthesised $SrTiO_3$ nanoparticles in different solvent medium. (A) H_2O, (B) H_2O/EG, C, H_2O/DEG, and D, H_2O/TMG. The volume ratio of H_2O/organic solvents for (B-D) was fixed to 43/57 (v/v). The scale bar in (A) is common for all images. Reproduced from Kimijima et al[25]

so formation of smaller nanoparticles that highly crystalline.[60]

In 2013, Nakashima et al[23] reported to synthesise $SrTiO_3$ nanoparticles by using a mixture of 2-methoxy ethanol as absolute alcohol as the solvent. It was found that the solvothermal technique is enabled to control the particle shape and size in the particular research effectively. Besides that, Kimijima et al[61] successfully synthesised $SrTiO_3$ particles in cubic, spherical, and flake-like shaped by using H_2O/polyols mixture solutions (eg, H_2O/EG, H_2O/DEG, and H_2O/TMG) as the medium for solvothermal reaction in the same year (Figure 5). It was found that, in order to maintain final particle shape and size, one of the competitive factors is the solvent effect of glycols.

2.3 | Solid-state reaction

In a normal synthesis reaction to take place, the precursors are placed in a solvent initially. Researchers are able to remove that yield from the solvent after the synthesis was done. For SSR, however, it enables the precursors to react chemically in the absence of the solvent. The elimination of solvents indicates that it will cost lesser for production; therefore, SSR gains attention in industries. In addition, eliminating the solvent also indicates that a SSR yields more final product than other synthesis methods. Since there is a "solventless" reaction, there is no waste to remove at final stage of preparation, thus, SSR also known as an environmentally friendly synthesis method. SSR can take place in several conditions. For example, oven method required higher temperatures to drive reactions without solvents whereas for melt method, the precursors are melted together. The melted precursors interact in the molten state and become a paste, which then hardens into a solid. In 2001, Berbenni et al[62] successfully synthesised $SrTiO_3$ nanoparticles by using conventional SSR; however, the particles were found to be large and nonuniform. In order to form a homogenous product, in recent, SSR usually incorporates with ball miller. In 2008, Liu et al[10] did a comparison by synthesising $SrTiO_3$ nanoparticles by using conventional SSR and ball milling reaction. For conventional SSR, the average nanoparticles diameter of $SrTiO_3$ was found to be in between 140 and 150 nm. Meanwhile, for ball milling–assisted SSR, it formed a smaller $SrTiO_3$ nanoparticle size (approximately 50 nm); however, the $SrTiO_3$ nanoparticles sample was found to be contaminated with metal during the synthesis process, and the photocatalytic activity is affected.[10] It was reported that the milling parameters can affect the lattice parameter, strain, and the grain size of the final product.[63,64] Therefore, the milling speed and time must be optimised in order to produce a desired morphology.

There are many advantages to develop the SSR. In common, $SrTiO_3$ for the applications in industry is produced by SSR with the precursor of TiO_2 and $SrCO_3$ because of the inexpensiveness of the precursors and simplicity of the production. Nonetheless, there are also some disadvantages such as the ideal process should produce a uniform or homogenous yield but some SSR does not. Furthermore, a high calcination temperature (>900°C) is required in this process causing many drawbacks of the final product such as high degree of nanoparticles agglomeration and large nanoparticles size with lacking uniformity. The high temperature is applied for the reaction to promote the rate of diffusion. Nevertheless, the high reaction temperatures can be difficult to combine ions that easily form volatile species and not possible to access the low temperature, metastable yields. The particles produced by this technique are not small enough; the efficiency is too low and cost much energy also the drawbacks of SSR. Thus, to develop an environmental friendly and practical pathway for the scale-up production of monodispersed $SrTiO_3$ nanoparticles at lower cost and temperature are important.

2.4 | Molten salt synthesis

Molten salt synthesis (MSR) is another technique to synthesis ceramic powders. This process involves using molten salt as the medium for synthesising complex oxides from their precursors. Some researchers attempted to use alkali halides as fluxes for crystal growth.[65,66] Basically, the function of flux is to improve the rate of SSR reaction as well as to promote crystallisation without using extreme temperature. Besides low temperature, the flux technique also provides one-step synthesis for a large number of oxides, solid solutions, and single crystals. In most cases, the purpose of eutectic mixture of salts is to promote liquid formation at lower temperature. For example, the temperatures to melt KCl and NaCl are 770°C and 801°C, respectively, but mixture of half KCl and NaCl (eutectic composition) was only 650°C. Molten salt plays some important role for synthesis,[67] which are (i) to enhance the rate of reaction and lower the temperature of reaction, (ii) to improve the degree of homogeneity (the precursors elements distribution in the solid solution), (iii) to control particle shape, (iv) to control particle size, and (v) to control the agglomeration.

Wang et al[19] successfully synthesised $SrTiO_3$ by MSR in 2011. On the basis of Wang et al,[19] TiO_2 and Sr

$(NO_3)_2$ were used as starting materials and NaCl-KCl was used as the molten salt flux. Under synthesis temperature of 700°C, 11 to 43 nm of $SrTiO_3$ was formed. In 2015, Zhang et al[28] synthesised the $SrTiO_3$ by using low temperature by using NaCl-H_2O assisted strategy. It was found that the NaCl-H_2O system able to facilitate the diffusivity of Sr precursor and TiO_2. By assisted of NaCl-H_2O, the reaction temperature was managed to reduce from 900°C to 750°C. As a result, the NaCl-H_2O system was able to offer a favourable medium to form $SrTiO_3$ nanoparticles at lower temperature.[28] However, it was reported that the drawback of this technique was the incorporation of impurities into the yields, which is a frequently observed phenomenon in the process of the flux treatment.[68] In 2016, Ham et al[32] studied the effects of $SrCl_2$ flux treatment on $SrTiO_3$. The $SrTiO_3$ synthesising reaction was taken place in a different crucible, which are alumina (Al) and yttrium (Y). Surprisingly, a small amount of Al and Y was doped into the $SrTiO_3$ compound and gives a better photocatalytic activity compared with the pristine $SrTiO_3$.

As solvent only, the salt melts should not be directly involved in the synthesis reaction. The separation the salt from the product at the final stage of synthesis was important. Basically, it was done by rinsing with water but a little quantity of salts can always be left over in the yields. This problem is not only related to the solubility of salts with water, but rather due to the intrinsic interactions between the salts and the product yields, which even can result in intercalates or solid solutions. This high interaction of the solvent with the yield is indeed one of the significant downsides of flux treatment synthesis that need to be look carefully in the quality control of the as-obtained yields.[69]

2.5 | Sonochemical

Sonochemistry is a technique for the nanoparticles preparation that has been gaining increased attention because of the extreme conditions that can be achieved which can result in unique reaction pathways and mechanisms.[70-72] In a sonochemical method, the reaction of the starting materials proceeds in the presence of high-frequency ultrasonic waves. Energy is applied to the system by irradiating a liquid with ultrasonic waves in high intensity for the purpose of produce regions of extreme pressure and temperature.[73] Ultrasound does not directly produce these extreme conditions because acoustic wavelengths are much larger than molecular dimensions and thus no direct molecular level interaction between chemical species and ultrasound occurs. In producing nanoparticles, sonochemical synthesis has several advantages.[70] On top of that, when using sonochemistry, no chemical reducing agent is needed. This is because the sonochemical irradiation of both organic solvents and water generates radicals, which can act as reducing agents. Also, because of the extreme conditions, the rate of reaction is reasonably rapid and very small nanoparticles are typically formed.

It was reported that the sonochemical method is usually used to control and improve the properties of the prepared photocatalyst, particularly its morphology and size, by generating ultrasonic waves. This method is widely applied for materials including alloys, oxides, colloids, and carbides.[59] In 2003, Yu et al[74] reported that the size control of the resulting $SrTiO_3$ is probably because of the viscosity in the solvent systems. During $SrTiO_3$ formation process, the competition between the nucleation and crystal growth is partially controlled by diffusion. The nanoparticles diffusion is harder to take place in high viscosity medium. Thus, this phenomenon favours the crystallisation and formation of new nuclei, which lead to smaller crystal size. Because EtOH (1.040 mPa.s at 25°C) has a higher viscosity than water (0.890 mPa.s at 25°C), therefore, solvent systems with higher EtOH contents would generate $SrTiO_3$ crystals in smaller nanoparticle size. In addition, higher viscosity of solution would result a weaker acoustic cavitation.[75] This may also cause in a decrease in the crystal size of $SrTiO_3$. In 2006, Xu et al[76] reported to synthesise $SrTiO_3$ nanoparticles using sonochemical method. The nanoparticle size of $SrTiO_3$ was in a ranging of 86 to 500 nm due to the nanoparticle size could be varied in different synthesis conditions such as the concentration of reactants, time, and sonication power. Besides that, it was found the $SrTiO_3$ nanoparticle shape was in spherical, cubic, and star-like. A similar finding was reported by another publication[30] in 2015 by using a lower temperature (50°C) of sonochemical synthesis. However, agglomeration was found on the basis of the field emission scanning electron microscopy (FESEM) analysis. Therefore, the synthesis condition is important in sonochemical reaction in order to produce a desired final product. Also, it was explained by Ashiri et al,[30] during the sonication process, ultrasonic waves radiate via starting materials solution causing alternating high and low pressure in the solution of starting materials. This causing the bubbles formation, growth, and implosive collapse in the solution. The collapsed bubbles with short lifetimes generate high pressure and intense local heating. On the basis of the hot spot theory,[77] extreme high temperatures (>5000 K) and pressures (approximately 1000 atm) are obtained upon the collapse of a bubble. Thus, the above-mentioned conditions highly accelerate the reaction rate without requiring any extra heating process.

2.6 | Sol-gel

The past 20 years, it was shown grow in number of interest in the materials development prepared by the sol-gel synthesis. The sol-gel method is a versatile process applied for producing a variety of oxide compounds. The process of sol-gel synthesis includes hydrolysis and condensation of the metal alkoxide followed by high temperature treatment that promotes polymerisation and finally becomes a metal oxide network. Generally, the sol-gel synthesis technique enables to control of the morphology, chemical properties, and the texture of the final products. This method also has a few merits over synthesis technique (eg, enabling impregnation of coprecipitation, which can be applied to introduce dopants). Although sol-gel is a popular pathway for nanomaterial synthesis, however, the metal alkoxides precursor might be expensive. Also, a high temperature of calcination is always required for the posttreatment in order to get the final product in crystalline form. A low temperature of calcination might lead to the final yields with defects, low crystallinity and finally affects the photocatalytic activity. Furthermore, in the experimental condition, a slight change would produce different catalyst properties of yield. As a result, the sol-gel process should be taken accurately and carefully when producing $SrTiO_3$ using this method. In 2001, a publication[78] was successfully prepared $SrTiO_3$ by using sol-gel synthesis technique. It was noticed that the crystallinity of the final product directly affected the E_g of $SrTiO_3$. High crystallinity of final product gives lower E_g that can relate to the photocatalytic activity. Meanwhile, for the poor crystallinity final product, it gives larger E_g compared with those single crystals. It was suspected that this is due to the quantum size effect and existence of amorphous phase in $SrTiO_3$.

The Pechini method builds on the theory of sol-gel chemistry involving small molecule chelating ligands in the preliminary step in order to promote a homogeneous solution of metal/citrate complexes formation. Nevertheless, the Pechini method takes this further to convert the mixture into a covalent polymer network to entrap the metal ions. This method is to delay the organic matrix decomposition in high temperature in order to afford more control over the growing ceramic product. In a typical process, a metal salt is dissolved in water with ethylene glycol and critic acid to form a homogeneous starting materials solution that contains metal-citrate chelate complexes. This solution was then heated to start the polyesterification process between the ethylene glycol and citrate, forming an extended covalent network. One of the major benefits of Pechini method was it can form a polymeric precursor where two metals or above may dispersed homogeneously throughout the network. Liu et al[10] synthesised $SrTiO_3$ by using both Pechini method and SSR. It was found that $SrTiO_3$ is that synthesised by Pechini method gives a smaller particle size (approximately 30 nm) as compared with SSR (approximately 150 nm). The $SrTiO_3$ that is synthesised by Pechini method also gives a uniform morphology and better in photocatalytic activity.

2.7 | Others

Besides the methods discussed in previous section, some other $SrTiO_3$ synthesis methods were also reported. Coprecipitation is a method that needs a metal cation from a common medium, coprecipitated usually as OH^-, CO_3^{2-}, $C_2O_4^{2-}$, or $C_3H_5O(COO)_3^{3-}$.[79-81] These precipitates are subsequently annealed at appropriate temperatures to produce the powder yields. In order to achieve high homogeneity, the solubility products of the metal cations precipitate should be close.[82] This procedure is unsuitable for the preparation of high purity and accurate stoichiometric phase. Coprecipitation results in atomic scale mixing, and hence, the temperature for annealing for the final product formation is low. This leads to lower nanoparticle size in the resulting multicomponent oxide powders.[83] In addition, coprecipitation route is necessary to control the stirring speed of the mixture, temperature, pH, and the concentration of the solution in terms of obtaining the final product with required properties.[84,85]

Combustion is a series of complex chemical reactions between an oxidant and a fuel together with the heat production and/or light in the form of either glow or flames. The combustion concept uses the art of fast thermal degradation of starting material chemicals by reacting with O_2; it has been effectively applied for the preparation of various nanoscale metal oxides.[86,87] This method contains some disadvantages such as contamination because of the carbonaceous residue, nanoparticles agglomeration, and no control on nanoparticles morphology. Understanding of combustion behaviour is required to perform the controlled combustion in order to get the yields with desired properties.

3 | APPLICATIONS OF $SrTiO_3$

3.1 | Photocatalysis

When the photons (light energy) fall on the semiconductor surface and if the energy of incident light is equivalent or greater than the band gap energy of the semiconductor, the electrons from valence band (VB) are exciting and jump to the semiconductor CB. $SrTiO_3$ is a semiconductor that has been well known to possess activity for photocatalysis. It has 3.2 eV of band gap that can produce

TABLE 3 The list photocatalysis applications for $SrTiO_3$

Photocatalyst	Applications and Uses	Light Source	Reference (Year)
Rh-$SrTiO_3$	PEC water splitting	300 W Xe lamp ($\lambda > 420$ nm)	[88] (2011)
$LaFeO_3$ thin films grown on Nb-$SrTiO_3$	PEC water splitting	300 W Xe lamp	[89] (2015)
rGO wrapped $SrTiO_3$ flower-like nanostructure	Hydrogen production from formic acid	N/A	[90] (2018)
$SrTiO_3$ anisotropic facets	Photochemical water splitting	300 W Xe lamp	[91] (2016)
$SrTiO_3/TiO_2$ NT	Photochemical water splitting	Simulated sunlight lamp (310 W/m^2, XHA500)	[92] (2016)
Ternary CdS/Au/3DOM-$SrTiO_3$	Photochemical water splitting	300 W Xe lamp	[93] (2017)
Facet functionalised $SrTiO_3$ (001) and (023)	Photochemical water splitting	500 W Xe lamp	[94] (2016)
CdSe/$SrTiO_3$ nanocomposites	Photochemical water splitting	300 W Xe lamp	[95] (2019)
$SrTiO_3$ grown on GaAs (001)	PEC water splitting	300 W Xe lamp	[96] (2017)
ZnO/$SrTiO_3$	Photochemical water splitting and fuel cell	300 W Xe lamp	[97] (2018)
$SrTiO_3$ nanocubes	PEC water splitting	100 W Hg lamp	[6] (2018)
$SrTiO_3/AgPO_4$	Photocatalytic water oxidation (O_2 production)	300 W Xe lamp ($\lambda > 420$ nm)	[98] (2014)
Ag/Fe_3O_4 bridged $SrTiO_3$/GCN	Photochemical water splitting and degradation of levofloxacin	300 W Xe lamp	[99] (2018)
Polythiophene/mp $SrTiO_3$	Degradation of methylene blue	250 W visible lamp	[100] (2018)
Mn-$SrTiO_3$ nanocubes	Degradation of tetracycline	250 W Xe lamp ($\lambda > 420$ nm)	[43] (2015)
$SrTiO_3$ nanocubes	Degradation of crystal violet	15 W 365 nm UV lamp	[7] (2014)
Cr-$SrTiO_3$ nanoplates	Cr (VI) removal	500 W Xe lamp ($\lambda > 420$ nm)	[101] (2019)
mp N-$SrTiO_3$	Degradation of methyl orange	400 W halogen lamp ($\lambda > 400$ nm)	[102] (2019)
$SrTiO_3/TiO_2$ nanosheets exposed (001) facets	Degradation of rhodamine B	300 W Xe lamp ($250 < \lambda < 380$ nm)	[103] (2014)
Bimodal-pore $SrTiO_3$ microspheres	Cr (VI) removal	500 W Xe lamp	[104] (2016)
$BiVO_4/SrTiO_3$ nanocomposites	Degradation of sulfamethoxazole	500 W Xe lamp	[105] (2017)
$TiO_2/SrTiO_3$ and $SrTiO_3$ microspheres (Rh, Ru, Pt decorated)	Phenol oxidation and degradation	UV-Vis light ($\lambda > 350$ nm)	[48] (2017)
Ag-$SrTiO_3$	Degradation of NO in air	300 W Xe lamp	[106] (2016)
$SrTiO_3$ (decorated with $SrCO_3$)	Degradation of NO in air	300 W Xe lamp ($\lambda > 420$ nm)	[107] (2018)
Cr-$SrTiO_3$	Degradation of NO in air	LED lamps 2 W/m^2 in different wavelengths (390, 445, 530, 627 nm)	[108] (2013)
Ag, F-$SrTiO_3$	Degradation of VOCs (Toluene)	300 W Xe lamp ($\lambda > 420$ nm)	[109] (2018)
Surface hydroxylation $SrTiO_3$	Degradation of VOCs (Toluene)	300 W Xe lamp ($300 < \lambda < 400$ nm)	[110] (2016)
Ag_3PO_4/Cr-$SrTiO_3$	Degradation of VOCs (Isopropanol)	300 W Xe lamp ($420 < \lambda < 800$ nm)	[111] (2013)
Carbon nitride polymer sensitisation and N-$SrTiO_3/TiO_2$ NT heterostructure	Degradation of VOCs (Toluene)	300 W Xe lamp	[112] (2017)
Cu_xO nanocluster loaded $SrTiO_3$ nanorod thin film	Reduction of CO_2 into CO (using H_2O)	Hg-Xe lamp	[113] (2016)
Rh-$SrTiO_3$	Reduction of CO_2 into CO (using H_2)	N/A	[114] (2018)
B-$SrTiO_3$	Reduction of CO_2 into CH_4	300 W Xe lamp	[115] (2017)
Cr-$SrTiO_3$	Reduction of CO_2 into CH_4	300 W Xe lamp ($\lambda > 420$ nm)	[116] (2015)

(Continues)

TABLE 3 (Continued)

Photocatalyst	Applications and Uses	Light Source	Reference (Year)
$SrTiO_3$	Reduction of CO_2 into CO (using H_2O)	300 W Xe lamp	[117] (2018)
Ag-$SrTiO_3$	Reduction of CO_2 into CO	300 W Xe lamp ($\lambda > 420$ nm)	[118] (2018)
$SrTiO_3$	Dye sensitised solar cell	N/A	[119] (2017)
$SrTiO_3$/ZnO nanocomposites	Dye sensitised solar cell	AM 1.5G (100 mW/cm^2)	[120] (2018)
TiO_2/$SrTiO_3$	Dye sensitised solar cell	AM 1.5G (100 mW/cm^2)	[121] (2015)
$SrTiO_3$	Dye sensitised photoelectrosynthesis cell	75 mW/cm^2 chopped light (445 nm)	[122] (2016)

Abbreviations: 3DOM, 3 dimensionally ordered macroporous; GCN, graphitic carbon nitride; mp, mesoporous; N/A, not available; NO, nitrogen oxide; NT, nanotubes; PEC, photoelectrochemical; rGO, reduced graphene oxide; VOCs, volatile organic compounds.

photogenerated charge carriers under irradiation of UV ($\lambda \leq 387.5$ nm). Therefore, $SrTiO_3$ was applied in several photocatalysis applications as listed in Table 3.

The CB edge of $SrTiO_3$ is lie at −0.61 eV, and the VB edge is lie at 2.59 eV.[123] Thus, $SrTiO_3$ is a suitable candidate for water splitting process due to its redox potential. Photocatalytic hydrogen production is look upon as a sustainable energy and environment friendly to generate alternative and green energy sources because the procedure is relatively easy and zero emission. A semiconductor, light energy, and water are the main resources for this procedure. The water splitting reaction is not a spontaneous process ($\Delta G = 237.178$ kJ/mol) under standard ambient pressure and temperature; it requires external energy to break the water molecule bonding, such as electricity.[124] In this case, $SrTiO_3$ act as photocatalyst to provide photogenerated electron-hole pairs to allow the redox reaction to take place. In 2008, Liu et al was tested the water splitting performance of pristine $SrTiO_3$ under irradiation of strong UV light.[10] Thereafter, Iwashina and Kudo successfully performed to split the water under visible light by modifying the $SrTiO_3$ with Rh dopant.[88] It was observed that the photocatalytic response of $SrTiO_3$ was extended to 540 nm after doping with Rh. After this, the modification of $SrTiO_3$ gained other researchers' attention. In 2016, Su, Huang, and Wey reported the efficiency of $SrTiO_3$/TiO_2 nanotube composites for water splitting. Nanotubes itself has some advantages, for example, its redox ability, high corrosion resistance, and good electronic delivery.[125,126] In this case, the $SrTiO_3$ and TiO_2 allow photogenerated electrons to shift from the $SrTiO_3$ CB to that of TiO_2. Conversely, photogenerated holes migrate from the VB of TiO_2 to that of $SrTiO_3$; this led to a good charge separation and improved the charge transfer of bulk-to-surface. Then, in 2016, another research was reported that certain $SrTiO_3$ facet has its own functions.[94] For example, $SrTiO_3$ single crystal (001) promoted active sites for photo-reduction whereas (023) facet offered active sites for photo-oxidation. There is not only water splitting process can produce hydrogen, in 2018, Guo et al attempted to generate hydrogen from formic acid decomposition with $SrTiO_3$ composites.[90] Basically, formic acid is able to decompose via both dehydrogenation (Equation 3) and dehydration process with the aid of photocatalyst (Equation 4). However, these processes are potentially producing CO_2 and CO as by-product. Furthermore, $SrTiO_3$ was also applied in water oxidation studies by Guan and Guo in 2014.[98]

$$HCOOH \rightarrow H_2 + CO_2, \quad (3)$$

$$HCOOH \rightarrow H_2O + CO. \quad (4)$$

Rapid industrialisation and exploitation of nonrenewable energy sources has not only led to their exhaustion but also led to the build-up of pollutants in the environment.[127] Apart from hydrogen production, $SrTiO_3$ can also be used for various kinds of advanced oxidation processes (AOPs). This process is preferred because no hazardous sludge is generated. This process is to produce high reactive species, namely, hydroxyl ($OH^{\cdot}$) and superoxide radicals ($O_2^{\cdot -}$) to oxidise the organic pollutants.[128] One of the critical environmental issues is the presence of organic dyes in aqueous environments. This is due to the low biodegradability and toxicity of organic dyes to aquatic life in such environments. Moreover, the pigment is able to attenuate the transmission of sunlight into water. So it can affect the aquatic plants, which finally disturb the aquatic ecosystem. In 2018, Faisal et al reported to use degrade industrial dye such as methylene blue (MB) by using mesoporous $SrTiO_3$ and composited with polythiophene (PTh).[100] PTh is a conducting polymer that can act as efficient sensitizers in photocatalyst due to the π-conjugated electron system, high absorption

coefficients, and significant electron-hole mobility.[129] It was reported that the efficiency of PTh-$SrTiO_3$ photocatalyst was highly improved because the excited electrons in lowest unoccupied molecular orbitals (LUMOs) of PTh can be migrate to the CB of $SrTiO_3$. Besides MB dye, there are also other researchers reported to treat other industrial dyes, for example, methyl orange (MO),[102] crystal violet (CV),[7] rhodamine B (RhB),[103] and even phenol oxidation.[48] According to a survey in 2015, an alarming total of 36 detectable antibiotics (such as lincomycin, chloramphenicols, macrolides, and tetracyclines [TCs]) existed in China, which was approximately 53 800 tons.[130] This has caused public anxiety about the unfavourable effects on human health and the proliferation of multiresistant bacterial strains that reduce the therapeutic potential of antibiotics.[131] Therefore, in the same year, Wu et al attempted to degrade TCs by using Mn-doped $SrTiO_3$. It was noticed that the TCs were able to degrade effectively under visible light and the light harvesting was improved. Then, in 2018, Kumar et al did an experiment in levofloxacin (LFC) degradation with Ag/Fe_3O_4 bridged $SrTiO_3/g\text{-}C_3N_4$ with superior performance[99]; it was able to fully degrade in 90 minutes. LFC is a popular antibiotic that belongs to fluoroquinolone family that used in treating severe bacterial infections.[132] $SrTiO_3$ also played the role in heavy metal reduction,[104] such as Cr (VI) reduce to Cr (III). In particular, $SrTiO_3$ has the higher capability for reduction than TiO_2 and can form a heterostructure with TiO_2 to boost the photogenerated carriers separation because $SrTiO_3$ has more negative CB energy compared with TiO_2.

$SrTiO_3$ can also apply for air pollutants treatment. Zhang et al did a nitrogen oxide (NO) removal by using Ag-$SrTiO_3$ in 2016.[106] In this case, the Ag provides the plasmonic effect to the photocatalyst. The surface of plasmonic nanostructure has electrons that can be strongly interacted with incident photons when the oscillating frequencies are matched and lead to the localised surface plasmon resonance (LSPR). Initially, the pristine $SrTiO_3$ was only managed to remove 10% of NO in 30 minutes. Nonetheless, with the Ag-$SrTiO_3$ photocatalyst, the performance was doubled. Apart from NO, Guo et al tested the performance of $SrTiO_3$ in volatile organic compounds (VOCs) degradation; the target pollutant was isopropanol. In 2016, Kong et al reported in toluene degradation with the hydroxylation $SrTiO_3$.[110] It was reported by the author, the low photodegradation performance towards organic compound is because of the reactive radical species amount like $OH^{\cdot}$ and $O_2^{\cdot-}$ is low. Therefore, the $SrTiO_3$ surface hydroxylation strategy was proposed by Kong, Rui, and Ji in order (i) to allow the photogenerated holes able to react with the adsorbed H_2O or surface hydroxyl groups to form $OH^{\cdot}$, the abundance of the surface hydroxyl groups can boost this reaction, act as a hole scavengers to form $OH^{\cdot}$, and promote the charge separation; and (ii) to allow the OH^- shift the $SrTiO_3$ surface energy band to a more negative level,[133] which promotes the adsorbed O_2 reduction to form $O_2^{\cdot-}$ (Figure 6).

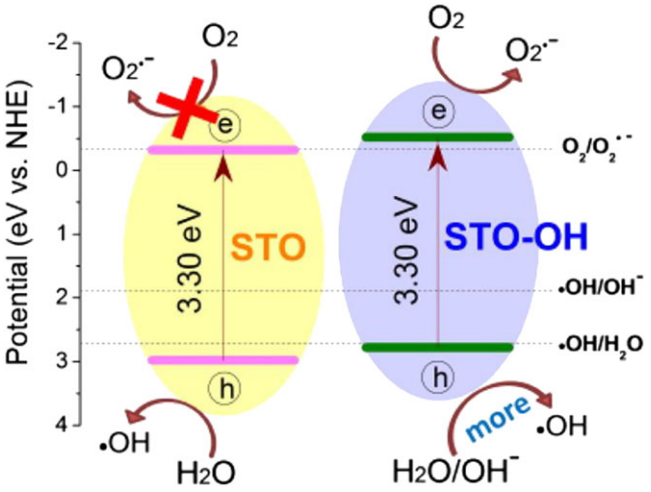

FIGURE 6 The energy band shifting of hydroxylation $SrTiO_3$ and pristine $SrTiO_3$. Reproduced from Kong et al[110] [Colour figure can be viewed at wileyonlinelibrary.com]

$SrTiO_3$ has sufficient negative CB for CO_2 reduction and high stability towards chemicals; thus, some scientist reported $SrTiO_3$ in CO_2 conversion. Photocatalytic CO_2 reduction is the process of CO_2 transformed into organic compounds (eg, CH_4, CH_3OH, HCOOH, and HCHO). In 2016, Shoji et al successfully converted the CO_2 into CO with $SrTiO_3$ composites. In this reaction, CO_2 is a very stable structure.[113] Thus, the role of $SrTiO_3$ is to produce photogenerated charge carriers. The electron at CB was to reduce the CO_2 structure; meanwhile, the holes at the VB were to oxidise the electron donor (H_2O). As the CO_2 photoreduction process proceeds via a multielectron process, for instance, four electrons are needed to produce HCHO (Equation 5), and eight electrons are required for CH_4 production (Equation 6). Therefore, the cocatalysts must gather photogenerated charge carriers at specific reaction sites to drive efficient CO_2 photoreduction. Apart from this, Yan et al also reported CO_2 reduction via reversed water gas shift (RWGS) reaction to produce CO,[114] and Shan et al published their work in CO_2 conversion to CH_4.[115]

$$CO_2 + 4\,H^+ + 4\,e^- \rightarrow HCHO + H_2O\ E_o = -0.48\ V\ vs\ NHE, \quad (5)$$

$$CO_2 + 8\,H^+ + 8\,e^- \rightarrow CH_4 + 2\,H_2O\ E_o = -0.24\ V\ vs\ NHE. \quad (6)$$

For dye-sensitised applications, $SrTiO_3$ was less studied by researchers compared with TiO_2. This is because

the TiO_2-based dye sensitised solar cell (DSSC) has been demonstrated as super-efficient at electron transportation, producing high photoconversion efficiency and high photocurrent density.[123,134,135] Moreover, frequently used inorganic dyes are functionalised with carboxylate or phosphate anchors that prone to adsorb better onto TiO_2 than $SrTiO_3$.[136,137] Despite of its weak properties, $SrTiO_3$ has been noted to present a CB potential more capable of unbiased proton reduction. Because of this, Gholamrezaei and Salavati-Niasari reported to perform DSSCs with $SrTiO_3$ photocatalyst; the photoconversion efficiency was determined to be 3.78%.[119] DSSCs are based on a semiconductor design coated in a dye that sensitive with light and surrounded by electrolyte, which is sandwiched between another electrolyte and a cathode. The anode is usually a material that transparent in order to allow the light transmission. $SrTiO_3$ is in the form of a mesh of particles suspended between the two electrodes. The light-sensitive dye is responsible to transform photons into electrons. The electrolyte is usually is I^- that helps in the transfer of electrons to cathode and vice versa. Then, in 2018, Banik et al attempted to use $SrTiO_3$/ZnO for the same application.[120] The reason to fabricate heterojunction photocatalyst was to prolong the charge carrier lifetime. In this time, the photoconversion efficiency was slightly better than the previous work,[119] which was 3.97%.

3.2 | Storage

$SrTiO_3$ can also apply in storage application (Table 4). MgH_2 is one of the most likely materials for the technology to store the hydrogen because of its high capacity in storage (7.6 wt%), relatively low raw material cost, superior reversibility, and high volumetric density. However, the bare MgH_2 has high onset dehydrogenation temperature, which is about 414°C. Therefore, Yahya and Ismail studied the effects of $SrTiO_3$ in MgH_2 for hydrogen storage.[138] It was found that $SrTiO_3$ in the $MgH_2/SrTiO_3$ composites was able to reduce the particle sizes. Initially, the particles size of MgH_2 was found to be 50 μm under FESEM analysis but the particle size managed to reduce to 1 μm after addition of $SrTiO_3$. This explained why the $MgH_2/SrTiO_3$ has lower temperature in dehydrogenation compared with the bare MgH_2. Smaller particle sizes have tendency to higher desorption and adsorption kinetics because of shorter hydrogen diffusion lengths, higher nucleation sites, and large specific surface areas.[150,151] As a result, $MgH_2/SrTiO_3$ was lowered down the onset temperature for dehydrogenation to 275°C in this particular research.

The development of energy storage devices is crucial to the present day and represents an exciting opportunity for innovation. Phase change materials (PCMs) are a class of substances that are capable of absorbing and releasing latent heat through phase transitions. PCMs can absorb large amounts of thermal energy at a certain temperature without getting hotter. In 2018, Pourmohamadian et al prepared $SrTiO_3$ microencapsulated palmitic acid (PA) for PCMs devices.[141] Pristine PA itself has a lower decomposition temperature, and the weight loss can be observed in between 170°C and 270°C. Thus, $SrTiO_3$ was encapsulated into PA in order to improve the stability. It was found that the weight-loss temperature increased to 240°C to 300°C for $SrTiO_3$ microencapsulated PA under analysis of thermogravimetric analyser.

Compared with battery storage, dielectric capacitors have high power density and ultra-fast charge/discharge speed. Hence, these capacitors are used widely in pulse power devices field, such as hybrid vehicles and mobile electronics; however, their energy density is also low.[152,153] $SrTiO_3$ belongs to linear dielectrics and possesses unique physical properties, such as moderate dielectric constant (approximately 300), relatively high breakdown strength (BDS), and low dielectric loss (<0.01).[143,154] It was reported that at the maximum fields, energy storage in the $SrTiO_3$ was about 30% higher than that in the $BaTiO_3$.[155] In 2014, Wang et al observed that the Sr/Ti ratio of $SrTiO_3$ would affect the energy storage properties.[144] It was found that the Sr/Ti ratio smaller than 1 exhibited higher BDS and energy density due to smaller grain sizes[156] while the Sr/Ti larger than 1 is prone to semiconductivity process. Before this, Tkach

TABLE 4 The list of storage applications for $SrTiO_3$

Material	Applications and Uses	Reference (Year)
$MgH_2/SrTiO_3$ (10 wt%)	Hydrogen storage	[138] (2019)
$MgH_2/SrTiO_3$/Ni	Hydrogen storage	[139] (2018)
$4MgH_2$-$Na_3AlH_6/SrTiO_3$	Hydrogen storage	[140] (2018)
$SrTiO_3$ microencapsulated palmitic acid	Thermal energy storage	[141] (2018)
$SrTiO_3/BiFeO_3$ thin films	Energy storage	[142] (2019)
$SrTiO_3$ with ZrO_2 additives	Energy storage	[143] (2014)
$SrTiO_3$ with different Sr/Ti mole ratios	Energy storage	[144] (2014)
BNT-ST-xBA	Energy storage	[145] (2019)
$SrTiO_3$ film	Energy storage	[146] (2017)
$SrTiO_3$−$Bi_{0.5}Na_{0.5}TiO_3$ −$BaAl_{0.5}Nb_{0.5}O_3$	Energy storage	[147] (2017)
$SrTiO_3$ thin film	Energy storage	[148] (2018)
$SrSn_xTi_{1-x}O_3$	Energy storage	[149] (2016)

Note: BNT-ST-xBA: $(1-x)(0.72Bi_{0.5}Na_{0.5}TiO_3$-$0.28SrTiO_3)$-$xBiAlO_3$.

et al also reported that Sr/Ti ratio can result in the changes of grain size and dielectric properties of $SrTiO_3$.[157] However, the $SrTiO_3$-based ceramics still yet to meet the practical applications due to relatively small recoverable energy storage density (W_{rec}) and maximum polarisation (P_{max}). Thus, Wang et al did another research in the same year by adding ZrO_2 additives into $SrTiO_3$.[143] It was found that when ZrO_2 additives increase, the grain size decreases and distribution becomes homogeneous, leading to the increase of the grain boundary thickness and the improvement of the BDS. By comparing with pure $SrTiO_3$, the energy was increased from 1.21 kJ/cm^3 to 1.62 J/cm^3, and the BDS was increased from 283 to 289 kV/cm.

3.3 | Sensors

Recently, semiconductor-based gas sensors made of perovskite oxides received interest because of the feasibility of doping with different metals to tailor their particular sensitivity.[158] There are two cations with different sizes in the perovskite structure that can be replaced by the various dopants. Furthermore, perovskite oxides are suitable for detecting gas (Table 5) in high temperature environment due to high melting point and high stability. In 2014, Chan et al conducted an experiment for hydrogen detection by using $SrTiO_3$ composites.[159] $LaAlO_3$ was composited with $SrTiO_3$ to form a heterostructure. It was found that $LaAlO_3$ layer results in significant changes in transport properties at the interface and has been studied by the recent first principle calculation and experimental work.[168,169] Then, in 2015, Schultz et al successfully substituted La in $SrTiO_3$ and act as a donor impurity at high temperature under reducing conditions, increasing the carrier concentration.[9,170,171] It was reported by other researchers that oxygen deficiency of $SrTiO_3$ is one of the most important modifying factors, doping of foreign elements can cause the change of optical and electrical properties.[172]

TABLE 5 The list of sensor applications for $SrTiO_3$

Material	Applications and Uses	Reference (Year)
La-$SrTiO_3$ films	Gas sensor for H_2	[9] (2015)
$LaAlO_3/SrTiO_3$	Gas sensor for H_2	[159] (2014)
SrTiO3-?	Gas sensor for ethanol	[160] (2017)
$SrTiO_3$ films	Gas sensor for ethanol	[161] (2010)
$SrTiO_3$/?-cyclodextrin composite	Detection of As (III)	[162] (2018)
$SrTiO_3$ decorated rGO	Detection of nitro-substituted aromatics	[163] (2016)
$TiO_2/SrTiO_3$ composite	Sensor for humidity	[164] (2017)
$SrTiO_3$ thin film	Thermal sensing	[165] (2019)
$SrTiO_3$	Microwave-based stress sensing	[166] (2018)
Branched TiO_2 NRs/$SrTiO_3$	Detection of biomarkers (alpha fetoprotein and cancer antigen 153)	[167] (2018)

Abbreviations: As (III), Arsenic (III); NRs, nanorods; rGO, reduced graphene oxide.

In 2016, Ahmad et al first conducted an experiment in nitro-substituted aromatics detection. The detection of nitroarmatics such as 2,4-trinitrophenol (TNP), 2,4-dinitrotoluene (2,4-DNT), and 2,4,6-trinitrotoluene (TNT) has grown security and environmental concerns because of threat of terrorist activities and their hazards have generated major demand for innovative, field-deployable tools for detecting explosives in a fast, sensitive, reliable, and simple manner.[173] Besides that, a derivative of phenol family such as p-nitrophenol (p-NP) is a product or intermediate, which produced during the degradation of pesticides like organo-phosphorus. Therefore, a highly reliable, efficient, highly sensitive, and robust sensor is desired for the detection of p-NP and their derivatives. Before this, most of the explosives detector was expensive,[174,175] lack of sensitivity, and selectivity. In order to reduce that cost, Ahmad et al use $SrTiO_3$ as a catalyst with reduced graphene oxides (rGOs). The rGO can exhibit several excellent properties, for example, high thermal and electrical conductivity, chemical stability, and electron mobility. With composite with metal oxides such as $SrTiO_3$, it can form a highly functional composite, which can accelerate the performances.[176-178]

Apart from that, Karthika et al reported in As (III) detection in water and human blood serum samples with $SrTiO_3$ and β-cyclodextrin (β-CD) composite.[162] $SrTiO_3$ itself has limitation in electrochemical field due to poor selectivity, sensitivity, and hard immobilisation on electrode surfaces. Therefore, β-CD was applied as $SrTiO_3$ composite in order to immobilise $SrTiO_3$ on electrode surface easily. It was reported that the $SrTiO_3$/β-CD was successfully function as As (III) detection in the presence of human blood serum as well as water. It was suggested that the present modified electrochemical sensor may be used for clinical applications.

3.4 | Fuel cell

Solid oxide fuel cell (SOFC) is a device for electrochemical energy conversion that able to generate electricity from fuel

directly, which prevents losses of intermediate energy conversion and attains much higher electric efficiency.[179] Porous Ni-yttrium-stabilised zirconia (Ni-YSZ) cermet was commonly used as the SOFC anode for up to 10 years due to inexpensive, high catalytic, and electrochemical activities. In order to achieve adequate current collection and catalytic activity, the content of Ni is normally above 35 vol% in order to allow the connecting path formation for the electron transport.[180] Nonetheless, Ni in the anode would be reoxidised and causes some situations for commercial SOFC such as system shutdown, fuel supply failure, seal leakage, and possibly even very high fuel utilisation.[181-184] Therefore, it is encouraged to develop alternative anode materials with enough stability for redox reaction, higher thermal compatibility, and comparable electrochemical performance as that of the Ni-YSZ cermet (Table 6).

It was reported that pure $SrTiO_3$ was unable be applied as anode material because the electrical conductivity is low. So donor-doped $SrTiO_3$ has been developed to improve the electrical conductivity under reducing conditions.[170] In 2017, Shen et al reported La-doped $SrTiO_3$ exhibits n-type semiconducting behaviour when it is donor-doped and/or exposed to atmosphere of reduction. According to Table 6, it was noticed that many scientists did research work on La-doped $SrTiO_3$ in this recent year. This is because La is a good donor dopant as the ionic radius of La^{3+} (1.32 Å) is close to Sr^{2+} (1.44 Å). Under oxidising conditions, the compensation occurs through the formation of Sr vacancies in the lattice, coupled with the formation of SrO layers within the structure. Meanwhile, under reducing conditions, Sr vacancies and SrO layers are eliminated, and the charge compensation of La^{3+} ions becomes electronic through the formation of electrons in the CB, in other words, conversion of Ti^{4+} to Ti^{3+}.[8] Then, in 2018, Singh et al first studied on Dy-doped $SrTiO_3$ because the ionic radius of Dy^{3+} (1.23 Å) is close to the Sr^{2+} too.[187] Besides that, Liu et al reported that reduced Dy-doped $SrTiO_3$ has high electronic conductivity, indicating that it can be considered as anodic material for SOFCs.[195]

TABLE 6 The list of fuel cell applications for $SrTiO_3$

Material	Applications and Uses	Reference (Year)
La-$SrTiO_3$	Anodic material in SOFC	[185] (2016)
La, Ni-$SrTiO_3$	Anodic material in SOFC	[186] (2015)
Dy-$SrTiO_3$	Anodic material in SOFC	[187] (2018)
La-$SrTiO_3$	Electrolyte in SOFC	[188] (2018)
La, Co-$SrTiO_3$	Anodic material in SOFC	[189] (2016)
La-$SrTiO_3$ with GDC and SSZ	Anodic material in SOFC	[190] (2016)
La-$SrTiO_3$	Anodic material in SOFC	[8] (2017)
$SrVO_3/SrTiO_3$	Anodic material in SOFC	[191] (2018)
$La_{0.2}Sr_{0.8}Ti_{0.9}Ni_{0.1}O_3$	Anodic material in SOFC	[192] (2017)
$La_{0.4}Sr_{0.6}O_3$	Anodic material in SOFC	[193] (2017)
Y-$SrTiO_3$	Anodic material in SOFC	[194] (2019)

Abbreviations: GDC, $Ce_{0.9}Gd_{0.1}O_2$; SOFC, solid oxide fuel cell; SSZ, $(Sc_2O_3)_{0.1}(CeO_2)_{0.01}(ZrO_2)_{0.89}$.

3.5 | Others

Besides the above stated applications, Table 7 listed some other applications for $SrTiO_3$. In 2011, Chen and Chen were tested the adsorption ability of $SrTiO_3$ for heavy metal removal.[200] It was reported that the nanoparticles of $SrTiO_3$ have the adsorption rate constant of 0.0036 min^{-1} with the adsorption capacity of 54.33 mg/g for Cu (II) removal. This indicates that the nanosized $SrTiO_3$ does not have rapid adsorption rate but it has a considerably large adsorption capacity. In 2016, Shahabuddin et al modified $SrTiO_3$ with polyaniline-

TABLE 7 The list of others applications for $SrTiO_3$

Material	Applications and Uses	Reference (Year)
$SrTiO_3$	Anode material for Li-ion batteries	[196] (2011)
Pt/$SrTiO_3$ nanocuboids	Propane oxidation	[197] (2011)
Co, Fe-$SrTiO_3$	Oxygen transport membranes	[198] (2018)
$SrTiO_3$ reinforced polyester resin/styrene blend	Study on dielectric property	[199] (2016)
$SrTiO_3$	Cu (II) adsorption	[200] (2011)
PANI-coated GO@$SrTiO_3$	Methyl orange and methylene blue adsorption	[201] (2016)
Rh-$SrTiO_3$	Inactivation of bacteriophage	[202] (2017)
$SrTiO_3/TiO_2$ nanotube	Biomedical applications	[203] (2015)
$SrTiO_3$	Capacitor applications	[204] (2018)
ITO/$LaAlO_3/SrTiO_3$	Memristor applications	[205] (2014)
Fe-$SrTiO_3$	Memristor applications	[206] (2010)
Amorphous $SrTiO_3$	Memristor applications	[207] (2014)
Flexibile butyl rubber $SrTiO_3$	Microwave applications	[208] (2011)
$SrTiO_3$ NT embedded Ag_2O	Osteogenic applications	[209] (2017)

Abbreviations: Cu (II), Copper (II); GO, graphene oxide; ITO, indium-doped tin oxide; PANI, polyaniline.

coated graphene oxide to form a composite structure (PANI-GO@$SrTiO_3$) for carcinogenic dyes adsorption.[201] that a synergistic phenomenon taking place between the PANI chain, GO sheets, and $SrTiO_3$. It was proposed that the fast adsorption was due to the ?-? interaction between the aromatic backbone of the dye and the aromatic skeleton of PANI-GO@$SrTiO_3$. Under reaction of 2 hours, it was successfully removed 96.5% of MB and 94.2% of MO, respectively. The $SrTiO_3$ was adhered to the sheets of GO through Sr^{3+} ions interactions with am sp^2 hybridised framework of GO. Thus, the role of $SrTiO_3$ in the composite structure was act as spacers that help in the segregation of GO sheets, thereby enhancing the total specific surface area.

Currently, the prevention of phage infection is limited to biological approaches, which are difficult to apply in an industrial setting. $SrTiO_3$ can also be used in biology applications. In 2017, Yamaguchi et al demonstrated Rh-doped $SrTiO_3$ for bacteriophage inactivation.[202] The pure $SrTiO_3$ does not exhibit photocatalytic activity under visible light irradiation. In recent years, Rh-doped $SrTiO_3$ has gain attention as a visible light-driven photocatalyst.[210,211] Under irradiation of visible light ($\lambda > 440$ nm), Yamaguchi et al noticed that Rh-doped $SrTiO_3$ showed selective inactivation of phage without bactericidal activity. After inactivation, the colour of Rh-doped $SrTiO_3$ was changed from grey to purple, suggesting that the valence state of dopant was partially changed from Rh^{3+} to Rh^{4+} induced by photocatalysis.

In 2011, Enterkin et al did a propane oxidation research by using Pt/$SrTiO_3$ nanocuboids.[197] $SrTiO_3$ was attractive for deep oxidation because of their good thermal stability, high bulk oxygen mobility, and their surface redox properties.[212,213] Nevertheless, in order to improve the oxidation activity, noble metals such as Pt and Pd were partially substituted into position B of the perovskite structure (ABO_3).

4 | CONCLUSIONS

In summary, $SrTiO_3$ gained many interests by scientists for miscellaneous applications such as photocatalysis, storage, sensor, and fuel cell because of its extraordinary properties. The synthesis method of $SrTiO_3$ was discussed in this article. It was found that the synthesis method and the ratio of precursors can affect the morphology, crystallinity, particle size, and shape of $SrTiO_3$. Hydrothermal and solvothermal synthesised $SrTiO_3$ can produce fine and uniform nanoparticles, but it is hard to apply for mass production. SSR is suitable for large-scale production, but the particles size and shape of synthesised $SrTiO_3$ might not regular, and it requires extreme temperatures. Thus, nowadays, some researchers were proposed to apply molten salt as a flux treatment in order to lower down the synthesis temperature. One of the major applications for $SrTiO_3$ was to produce hydrogen fuel via photocatalysis process.[214] This is because the band gap of $SrTiO_3$ was tunable, and it is thermal and chemical stable under photocatalytic reaction.

ACKNOWLEDGEMENTS

The authors greatly acknowledged the support of Prototype Research Grant Scheme (PR002-2016A) from Ministry of Education Malaysia and also SATU grant (ST010-2017) from University of Malaya.

ORCID

Wei-Hsin Chen https://orcid.org/0000-0001-5009-3960

REFERENCES

1. Chen P, Cosgriff MP, Zhang Q, et al. Field-dependent domain distortion and interlayer polarization distribution in PbTiO 3/SrTiO 3 superlattices. *Phys Rev Lett*. 2013;110(4):047601.
2. Neaton J, Rabe K. Theory of polarization enhancement in epitaxial BaTiO 3/SrTiO 3 superlattices. *Appl Phys Lett*. 2003;82(10):1586-1588.
3. Ekuma CE, Jarrell M, Moreno J, Bagayoko D. First principle electronic, structural, elastic, and optical properties of strontium titanate. *AIP Adv*. 2012;2(1):012189.
4. Liu ZQ, Leusink DP, Wang X, et al. Metal-insulator transition in SrTiO 3^{-} × thin films induced by frozen-out carriers. *Phys Rev Lett*. 2011;107(14):146802.
5. Yousefi R, Jamali-Sheini F, Cheraghizade M, et al. Enhanced visible-light photocatalytic activity of strontium-doped zinc oxide nanoparticles. *Mater Sci Semicond Process*. 2015;32:152-159.
6. Phoon BL, Lai CW, Pan GT, Yang TCK, Juan JC. One-pot hydrothermal synthesis of strontium titanate nanoparticles photoelectrode using electrophoretic deposition for enhancing photoelectrochemical water splitting. *Ceram Int*. 2018;44(8):9923-9933.
7. Huang S-T, Lee WW, Chang JL, Huang WS, Chou SY, Chen CC. Hydrothermal synthesis of SrTiO3 nanocubes: characterization, photocatalytic activities, and degradation pathway. *J Taiwan Inst Chem Eng*. 2014;45(4):1927-1936.
8. Shen X, Kawabata T, Sasaki K. Redox-stable Sr0. 9La0. 1TiO3-supported SOFC single cells. *Int J Hydrogen Energy*. 2017;42(10):6941-6949.
9. Schultz AM, Brown TD, Ohodnicki PR Jr. Optical and chemiresistive sensing in extreme environments: La-doped SrTiO3 films for hydrogen sensing at high temperatures. *J Phys Chem C*. 2015;119(11):6211-6220.

10. Liu Y, Xie L, Li Y, et al. Synthesis and high photocatalytic hydrogen production of SrTiO3 nanoparticles from water splitting under UV irradiation. *J Power Sources*. 2008;183(2):701-707.
11. Chen Y-H, Chen Y-D. Kinetic study of Cu (II) adsorption on nanosized BaTiO 3 and SrTiO 3 photocatalysts. *J Hazard Mater*. 2011;185(1):168-173.
12. Souza AE, Santos GTA, Barra BC, et al. Photoluminescence of SrTiO3: influence of particle size and morphology. *Cryst Growth Des*. 2012;12(11):5671-5679.
13. Rabuffetti FA, Kim HS, Enterkin JA, et al. Synthesis-dependent first-order Raman scattering in SrTiO3 nanocubes at room temperature. *Chem Mater*. 2008;20(17):5628-5635.
14. Liu S, Xiu Z, Liu JA, et al. Combustion synthesis and characterization of perovskite SrTiO 3 nanopowders. *J Alloys Compd*. 2008;457(1):L12-L14.
15. Chen L, Zhang S, Wang L, Xue D, Yin S. Preparation and photocatalytic properties of strontium titanate powders via sol–gel process. *J Cryst Growth*. 2009;311(3):746-748.
16. Li H-L, du ZN, Wang GL, Zhang YC. Low temperature molten salt synthesis of SrTiO 3 submicron crystallites and nanocrystals in the eutectic NaCl–KCl. *Mater Lett*. 2010;64(3):431-434.
17. Malghe Y. Nanosized SrTiO3 powder from oxalate precursor microwave aided synthesis and thermal characterization. *J Therm Anal Calorim*. 2010;102(3):831-836.
18. Sulaeman U, Yin S, Sato T. Solvothermal synthesis and photocatalytic properties of nitrogen-doped SrTiO 3 nanoparticles. *J Nanomater*. 2010;2010:32.
19. Wang TX, Liu SZ, Chen J. Molten salt synthesis of SrTiO 3 nanocrystals using nanocrystalline TiO 2 as a precursor. *Powder Technol*. 2011;205(1):289-291.
20. Moreira ML, Longo VM, Avansi W Jr, et al. Quantum mechanics insight into the microwave nucleation of SrTiO3 nanospheres. *J Phys Chem C*. 2012;116(46):24792-24808.
21. Yu H, Yan S, Li Z, Yu T, Zou Z. Efficient visible-light-driven photocatalytic H_2 production over Cr/N-codoped $SrTiO_3$. *Int J Hydrogen Energy*. 2012;37(17):12120-12127.
22. Kalyani V, Vasile BS, Ianculescu A, Buscaglia MT, Buscaglia V, Nanni P. Hydrothermal synthesis of $SrTiO_3$ mesocrystals: single crystal to mesocrystal transformation induced by topochemical reactions. *Cryst Growth Des*. 2012;12(9):4450-4456.
23. Nakashima K, Kera M, Fujii I, Wada S. A new approach for the preparation of SrTiO 3 nanocubes. *Ceram Int*. 2013;39(3):3231-3234.
24. Klaytae T, Panthong P, Thountom S. Preparation of nanocrystalline SrTiO 3 powder by sol–gel combustion method. *Ceram Int*. 2013;39:S405-S408.
25. Kimijima T, Kanie K, Nakaya M, Muramatsu A. Solvothermal synthesis of SrTiO 3 nanoparticles precisely controlled in surface crystal planes and their photocatalytic activity. *Appl Catal Environ*. 2014;144:462-467.
26. Hao Y, Wang X, Li L. Highly dispersed SrTiO 3 nanocubes from a rapid sol-precipitation method. *Nanoscale*. 2014;6(14):7940-7946.
27. Mourão HA, Lopes OF, Ribeiro C, Mastelaro VR. Rapid hydrothermal synthesis and pH-dependent photocatalysis of strontium titanate microspheres. *Mater Sci Semicond Process*. 2015;30:651-657.
28. Zhang J, Huang M, Yanagisawa K, Yao S. NaCl–H 2 O-assisted preparation of SrTiO 3 nanoparticles by solid state reaction at low temperature. *Ceram Int*. 2015;41(4):5439-5444.
29. Hou D, Hu X, Ho W, Hu P, Huang Y. Facile fabrication of porous Cr-doped SrTiO 3 nanotubes by electrospinning and their enhanced visible-light-driven photocatalytic properties. *J Mater Chem A*. 2015;3(7):3935-3943.
30. Ashiri R, Ajami R, Moghtada A. Sonochemical synthesis of $SrTiO_3$ nanocrystals at low temperature. *Int J Appl Ceram Technol*. 2015;12(S2):E202-E206.
31. Lee D, Vu H, Sun H, et al. Growth of (Na 0.5 Bi 0.5) TiO 3-SrTiO 3 single crystals by solid state crystal growth. *Ceram Int*. 2016;42(16):18894-18901.
32. Ham Y, Hisatomi T, Goto Y, et al. Flux-mediated doping of SrTiO 3 photocatalysts for efficient overall water splitting. *J Mater Chem A*. 2016;4(8):3027-3033.
33. Zhao W, Liu N, Wang H, Mao L. Sacrificial template synthesis of core-shell $SrTiO_3/TiO_2$ heterostructured microspheres photocatalyst. *Ceram Int*. 2017;43(6):4807-4813.
34. Subha N, M. M, Myilsamy M, et al. Influence of synthesis conditions on the photocatalytic activity of mesoporous Ni doped $SrTiO_3/TiO_2$ heterostructure for H_2 production under solar light irradiation. *Colloids Surf A Physicochem Eng Asp*. 2017;522:193-206.
35. Zhang Y, Zhong L, Duan D. Single-step hydrothermal synthesis of strontium titanate nanoparticles from crystalline anatase titanium dioxide. *Ceram Int*. 2015;41(10):13516-13524.
36. Zhang S, Liu J, Han Y, Chen B, Li X. Formation mechanisms of SrTiO 3 nanoparticles under hydrothermal conditions. *Mater Sci Eng B*. 2004;110(1):11-17.
37. Tsumura T, Matsuoka K, Toyoda M. Formation and annealing of BaTiO 3 and SrTiO 3 nanoparticles in KOH solution. *J Mater Sci Technol*. 2010;26(1):33-38.
38. Zhao W, Zhao W, Zhu G, Lin T, Xu F, Huang F. Black strontium titanate nanocrystals of enhanced solar absorption for photocatalysis. *CrstEngComm*. 2015;17(39):7528-7534.
39. Jayabal P, Sasirekha V, Mayandi J, Jeganathan K, Ramakrishnan V. A facile hydrothermal synthesis of SrTiO 3 for dye sensitized solar cell application. *J Alloys Compd*. 2014;586:456-461.
40. Karaphun A, Hunpratub S, Swatsitang E. Effect of annealing on magnetic properties of Fe-doped SrTiO 3 nanopowders prepared by hydrothermal method. *Microelectron Eng*. 2014;126:42-48.
41. Niishiro R, Tanaka S, Kudo A. Hydrothermal-synthesized SrTiO 3 photocatalyst codoped with rhodium and antimony with visible-light response for sacrificial H 2 and O 2 evolution and application to overall water splitting. *Appl Catal Environ*. 2014;150:187-196.
42. Yu H, Wang J, Yan S, Yu T, Zou Z. Elements doping to expand the light response of $SrTiO_3$. *J Photochem Photobiol A Chem*. 2014;275:65-71.
43. Wu G, Li P, Xu D, et al. Hydrothermal synthesis and visible-light-driven photocatalytic degradation for tetracycline of Mn-doped $SrTiO_3$ nanocubes. *Appl Surf Sci*. 2015;333:39-47.

44. Wang Y, Zhu L, Gao F, Xie H. Preparation, characterization and photocatalytic activities of TiO_2-$SrTiO_3$ composites. In: *IOP Conference Series: Materials Science and Engineering*. IOP Publishing; 2017.
45. Yin L, Zhou J, Gao L, et al. Characterization and osteogenic activity of $SrTiO_3$/TiO_2 nanotube heterostructures on microporous titanium. *Surf Coat Technol*. 2017;330:121-130.
46. Kiss B, Manning TD, Hesp D, et al. Nano-structured rhodium doped $SrTiO_3$–visible light activated photocatalyst for water decontamination. *Appl Catal Environ*. 2017;206:547-555.
47. Wang J, Zhang BY, Kang HJ, et al. Record high thermoelectric performance in bulk $SrTiO_3$ via nano-scale modulation doping. *Nano Energy*. 2017;35:387-395.
48. Grabowska E, Marchelek M, Klimczuk T, Lisowski W, Zaleska-Medynska A. TiO_2/$SrTiO_3$ and $SrTiO_3$ microspheres decorated with Rh, Ru or Pt nanoparticles: highly UV–vis responsible photoactivity and mechanism. *J Catal*. 2017;350:159-173.
49. Kobayashi M, Suzuki Y, Goto T, et al. Low-temperature hydrothermal synthesis and characterization of $SrTiO_3$ photocatalysts for NOx degradation. *J Cerma Soc Jpn*. 2018;126(2):135-138.
50. Crosby LA, Chen BR, Kennedy RM, et al. All roads lead to TiO_2: TiO_2-rich surfaces of barium and strontium titanate prepared by hydrothermal synthesis. *Chem Mater*. 2018;30(3):841-846.
51. Zhang H, Zhu Y, Li Z, Fan P, Ma W, Xie B. High discharged energy density of polymer nanocomposites containing paraelectric $SrTiO_3$ nanowires for flexible energy storage device. *J Alloys Compd*. 2018;744:116-123.
52. Lin H-Y, Cian L-T. Microwave-Assisted Hydrothermal Synthesis of $SrTiO_3$: Rh for Photocatalytic Z-scheme Overall Water Splitting. *Applied Sciences*. 2019;9(1):55.
53. Shen H, Lu Y, Wang Y, et al. Low temperature hydrothermal synthesis of $SrTiO_3$ nanoparticles without alkali and their effective photocatalytic activity. *J Adv Ceram*. 2016;5(4):298-307.
54. Lencka MM, Riman RE. Thermodynamic modeling of hydrothermal synthesis of ceramic powders. *Chem Mater*. 1993;5(1):61-70.
55. Douglas AS. *Fundamentals of Analytical Chemistry*. California, USA: Grupo Editorial Norma; 2004.
56. Moreira M, Mambrini GP, Volanti DP, et al. Hydrothermal microwave: a new route to obtain photoluminescent crystalline $BaTiO_3$ nanoparticles. *Chem Mater*. 2008;20(16):5381-5387.
57. Bilecka I, Niederberger M. Microwave chemistry for inorganic nanomaterials synthesis. *Nanoscale*. 2010;2(8):1358-1374.
58. Zhu X, Wang J, Zhang Z, et al. Perovskite nanoparticles and nanowires: microwave–hydrothermal synthesis and structural characterization by high-resolution transmission electron microscopy. *J Am Ceram Soc*. 2008;91(8):2683-2689.
59. Wang Y, He Y, Lai Q, Fan M. Review of the progress in preparing nano TiO 2: an important environmental engineering material. *J Environ Sci*. 2014;26(11):2139-2177.
60. Lucky RA, Sui R, Lo JMH, Charpentier PA. Effect of solvent on the crystal growth of one-dimensional ZrO_2− TiO_2 nanostructures. *Cryst Growth Des*. 2010;10(4):1598-1604.
61. Kimijima T, Kanie K, Nakaya M, Muramatsu A. Solvothermal synthesis of shape-controlled perovskite $MTiO_3$ (M= Ba, Sr, and Ca) particles in H_2O/polyols mixed solutions. *Mater Trans*. 2014;55(1):147-153.
62. Berbenni V, Marini A, Bruni G. Effect of mechanical activation on the preparation of SrTiO 3 and Sr 2 TiO 4 ceramics from the solid state system SrCO 3–TiO 2. *J Alloys Compd*. 2001;329(1):230-238.
63. Ahamed H, Kumar VS. A comparative study on the milling speed for the synthesis of nano-structured Al 6063 alloy powder by mechanical alloying. *J Miner Mater Charact Eng*. 2011;10(06):507-515.
64. Xu C, de S, Balu AM, Ojeda M, Luque R. Mechanochemical synthesis of advanced nanomaterials for catalytic applications. *Chem Commun*. 2015;51(31):6698-6713.
65. Ru X, Ma B, Huang J, Huang Y. Phosphogypsum transition to α-calcium sulfate hemihydrate in the presence of omongwaite in NaCl solutions under atmospheric pressure. *J Am Ceram Soc*. 2012;95(11):3478-3482.
66. Zhang Z, Wimbush SC, Kursumovic A, Suo H, MacManus-Driscoll JL. Detailed study of the process of biomimetic formation of YBCO platelets from nitrate salts in the presence of the biopolymer Dextran and a molten NaCl flux. *Cryst Growth Des*. 2012;12(11):5635-5642.
67. Kimura T. *Molten Salt Synthesis of Ceramic Powders, in Advances in Ceramics-Synthesis and Characterization, Processing and Specific Applications*. London, UK: InTech; 2011.
68. Muller G, Ostrogorsky A. *Handbook of Crystal Growth*. Oxford, UK: 2 Basic Techniques; 1994.
69. Liu X, Fechler N, Antonietti M. Salt melt synthesis of ceramics, semiconductors and carbon nanostructures. *Chem Soc Rev*. 2013;42(21):8237-8265.
70. Gedanken A. Using sonochemistry for the fabrication of nanomaterials. *Ultrason Sonochem*. 2004;11(2):47-55.
71. Fernando KS, Smith MJ, Harruff BA, Lewis WK, Guliants EA, Bunker CE. Sonochemically assisted thermal decomposition of alane N, N-dimethylethylamine with titanium (Iv) isopropoxide in the presence of oleic acid to yield air-stable and size-selective aluminum core−shell nanoparticles. *J Phys Chem C*. 2008;113(2):500-503.
72. Lewis WK, Rosenberger AT, Gord JR, et al. Multispectroscopic (FTIR, XPS, and TOFMS− TPD) investigation of the core−shell bonding in sonochemically prepared aluminum nanoparticles capped with oleic acid. *J Phys Chem C*. 2010;114(14):6377-6380.
73. Bang JH, Suslick KS. Applications of ultrasound to the synthesis of nanostructured materials. *Adv Mater*. 2010;22(10):1039-1059.
74. Yu JC, Zhang L, Li Q, Kwong KW, Xu AW, Lin J. Sonochemical preparation of nanoporous composites of titanium oxide and size-tunable strontium titanate crystals. *Langmuir*. 2003;19(18):7673-7675.
75. Mason T. *Practical Sonochemistry User's Guide to Application in Chemistry and Chemical Engineering*. UK: Ellis Horwood; 1991.
76. Xu M, Lu YN, Liu YF, Shi SZ, Fang F. Synthesis of monosized strontium titanate particles with tailored morphologies. *J Am Ceram Soc*. 2006;89(12):3631-3634.

77. Mason TJ, Lorimer JP. *Applied sonochemistry: The uses of power ultrasound in chemistry and processing*. Wiley-VCH Verlag, GmbH & Co. KgaA; 2002;1-48.
78. Bao D, Yao X, Wakiya N, Shinozaki K, Mizutani N. Band-gap energies of sol-gel-derived SrTiO 3 thin films. *Appl Phys Lett*. 2001;79(23):3767-3769.
79. Zhang Y, Cao H, Zhang J, Xia B. Synthesis of LiNi 0.6 Co 0.2 Mn 0.2 O 2 cathode material by a carbonate co-precipitation method and its electrochemical characterization. *Solid State Ion*. 2006;177(37):3303-3307.
80. Cho T-H, Shiosaki Y, Noguchi H. Preparation and characterization of layered LiMn 1/3 Ni 1/3 Co 1/3 O 2 as a cathode material by an oxalate co-precipitation method. *J Power Sources*. 2006;159(2):1322-1327.
81. Godinho M, Gonçalves RF, Santos LS, Varela JA, Longo E, Leite ER. Room temperature co-precipitation of nanocrystalline CeO 2 and Ce 0.8 Gd 0.2 O 1.9− δ powder. *Mater Lett*. 2007;61(8):1904-1907.
82. West AR. *Solid State Chemistry and Its Applications*. John Wiley & Sons; 2007.
83. Gaikwad AB, Navale SC, Samuel V, Murugan AV, Ravi V. A co-precipitation technique to prepare BiNbO 4, MgTiO 3 and Mg 4 Ta 2 O 9 powders. *Mater Res Bull*. 2006;41(2):347-353.
84. Jian-feng H, Xie-rong Z, Li-yun C, Xin-bo X. Preparation of Y 2 BaCuO 5 nanoparticles by a co-precipitation process with the aid of ultrasonic irradiation. *J Mater Process Technol*. 2009;209(6):2963-2966.
85. Xu G, Zhang X, He W, Liu H, Li H, Boughton RI. Preparation of highly dispersed YAG nano-sized powder by co-precipitation method. *Mater Lett*. 2006;60(7):962-965.
86. Biswas M, Prabhakaran K, Gokhale NM, Sharma SC. Synthesis of nanocrystalline yttria doped ceria powder by urea–formaldehyde polymer gel auto-combustion process. *Mater Res Bull*. 2007;42(4):609-617.
87. Jeong SK, Nahm KS, Stephan AM. Synthesis of Li (Co 0.8 Ni 0.2− y Al y) O 2 (y≤ 0.02) by combustion method as a possible cathode material for lithium batteries. *Mater Sci Eng A*. 2007;445:657-662.
88. Iwashina K, Kudo A. Rh-doped $SrTiO_3$ photocatalyst electrode showing cathodic photocurrent for water splitting under visible-light irradiation. *J Am Chem Soc*. 2011;133(34):13272-13275.
89. May KJ, Fenning DP, Ming T, et al. Thickness-dependent photoelectrochemical water splitting on ultrathin $LaFeO_3$ films grown on Nb: $SrTiO_3$. *J Phys Chem Lett*. 2015;6(6):977-985.
90. Guo M, Liu Q, Wu M, Lv T, Jia L. Novel reduced graphene oxide wrapped-$SrTiO_3$ flower-like nanostructure with Ti–C bond for free noble metal decomposition of formic acid to hydrogen. *Chem Eng J*. 2018;334:1886-1896.
91. Mu L, Zhao Y, Li A, et al. Enhancing charge separation on high symmetry SrTiO 3 exposed with anisotropic facets for photocatalytic water splitting. *Energ Environ Sci*. 2016;9(7):2463-2469.
92. Su E-C, Huang B-S, Wey M-Y. Enhanced optical and electronic properties of a solar light-responsive photocatalyst for efficient hydrogen evolution by $SrTiO_3/TiO_2$ nanotube combination. *Sol Energy*. 2016;134:52-63.
93. Chang Y, Yu K, Zhang C, et al. Ternary CdS/Au/3DOM-$SrTiO_3$ composites with synergistic enhancement for hydrogen production from visible-light photocatalytic water splitting. *Appl Catal Environ*. 2017;215:74-84.
94. Wang B, Shen S, Guo L. Surface reconstruction of facet-functionalized $SrTiO_3$ nanocrystals for photocatalytic hydrogen evolution. *ChemCatChem*. 2016;8(4):798-804.
95. Han J, Dai F, Liu Y, Zhao R, Wang L, Feng S. Synthesis of CdSe/$SrTiO_3$ nanocomposites with enhanced photocatalytic hydrogen production activity. *Appl Surf Sci*. 2019;467:1033-1039.
96. Kornblum L, Fenning DP, Faucher J, et al. Solar hydrogen production using epitaxial SrTiO 3 on a GaAs photovoltaic. *Energ Environ Sci*. 2017;10(1):377-382.
97. Wu Y, Dong B, Zhang J, Song H, Yan C. The synthesis of ZnO/$SrTiO_3$ composite for high-efficiency photocatalytic hydrogen and electricity conversion. *Int J Hydrogen Energy*. 2018.
98. Guan X, Guo L. Cocatalytic effect of $SrTiO_3$ on Ag_3PO_4 toward enhanced photocatalytic water oxidation. *ACS Catal*. 2014;4(9):3020-3026.
99. Kumar A, Rana A, Sharma G, et al. High-performance photocatalytic hydrogen production and degradation of levofloxacin by wide spectrum-responsive Ag/Fe_3O_4 bridged $SrTiO_3$/g-C_3N_4 plasmonic nanojunctions: joint effect of Ag and Fe_3O_4. *ACS Appl Mater Interfaces*. 2018;10(47):40474-40490.
100. Faisal M, Harraz FA, Ismail AA, et al. Polythiophene/mesoporous $SrTiO_3$ nanocomposites with enhanced photocatalytic activity under visible light. *Sep Purif Technol*. 2018;190:33-44.
101. Yang D, Zhao X, Zou X, Zhou Z, Jiang Z. Removing Cr (VI) in water via visible-light photocatalytic reduction over Cr-doped $SrTiO_3$ nanoplates. *Chemosphere*. 2019;215:586-595.
102. Atkinson I, Parvulescu V, Pandele Cusu J, et al. Influence of preparation method and nitrogen (N) doping on properties and photo-catalytic activity of mesoporous $SrTiO_3$. *J Photochem Photobiol A Chem*. 2019;368:41-51.
103. Yue X, Zhang J, Yan F, Wang X, Huang F. A situ hydrothermal synthesis of $SrTiO_3/TiO_2$ heterostructure nanosheets with exposed (0 0 1) facets for enhancing photocatalytic degradation activity. *Appl Surf Sci*. 2014;319:68-74.
104. Yang D, Sun Y, Tong Z, Nan Y, Jiang Z. Fabrication of bimodal-pore $SrTiO_3$ microspheres with excellent photocatalytic performance for Cr (VI) reduction under simulated sunlight. *J Hazard Mater*. 2016;312:45-54.
105. Li J, Wang F, Meng L, Han M, Guo Y, Sun C. Controlled synthesis of $BiVO_4/SrTiO_3$ composite with enhanced sunlight-driven photofunctions for sulfamethoxazole removal. *J Colloid Interface Sci*. 2017;485:116-122.
106. Zhang Q, Huang Y, Xu L, Cao JJ, Ho W, Lee SC. Visible-light-active plasmonic Ag–$SrTiO_3$ nanocomposites for the degradation of NO in air with high selectivity. *ACS Appl Mater Interfaces*. 2016;8(6):4165-4174.
107. Jin S, Dong G, Luo J, Ma F, Wang C. Improved photocatalytic NO removal activity of $SrTiO_3$ by using $SrCO_3$ as a new co-catalyst. *Appl Catal Environ*. 2018;227:24-34.

108. Li H, Yin S, Wang Y, Sekino T, Lee SW, Sato T. Roles of Cr_3+ doping and oxygen vacancies in $SrTiO_3$ photocatalysts with high visible light activity for NO removal. *J Catal*. 2013;297:65-69.
109. Ji W, Shen T, Kong J, Rui Z, Tong Y. Synergistic performance between visible-light photocatalysis and thermocatalysis for VOCs oxidation over robust Ag/F-codoped $SrTiO_3$. *Ind Eng Chem Res*. 2018;57(38):12766-12773.
110. Kong J, Rui Z, Ji H. Enhanced photocatalytic mineralization of gaseous toluene over $SrTiO_3$ by surface hydroxylation. *Ind Eng Chem Res*. 2016;55(46):11923-11930.
111. Guo J, Ouyang S, Li P, Zhang Y, Kako T, Ye J. A new heterojunction Ag_3PO_4/Cr-$SrTiO_3$ photocatalyst towards efficient elimination of gaseous organic pollutants under visible light irradiation. *Appl Catal Environ*. 2013;134:286-292.
112. Kong J, Rui Z, Ji H. Carbon nitride polymer sensitization and nitrogen doping of $SrTiO_3$/TiO_2 nanotube heterostructure toward high visible light photocatalytic performance. *Ind Eng Chem Res*. 2017;56(36):9999-10008.
113. Shoji S, Yin G, Nishikawa M, Atarashi D, Sakai E, Miyauchi M. Photocatalytic reduction of CO_2 by CuxO nanocluster loaded $SrTiO_3$ nanorod thin film. *Chem Phys Lett*. 2016;658:309-314.
114. Yan B, Wu Q, Cen J, et al. Highly active subnanometer Rh clusters derived from Rh-doped $SrTiO_3$ for CO_2 reduction. *Appl Catal Environ*. 2018;237:1003-1011.
115. Shan J, Raziq F, Humayun M, et al. Improved charge separation and surface activation via boron-doped layered polyhedron $SrTiO_3$ for co-catalyst free photocatalytic CO_2 conversion. *Appl Catal Environ*. 2017;219:10-17.
116. Bi Y, Ehsan MF, Huang Y, Jin J, He T. Synthesis of Cr-doped $SrTiO_3$ photocatalyst and its application in visible-light-driven transformation of CO_2 into CH_4. *J CO_2 Util*. 2015;12:43-48.
117. Luo C, Zhao J, Li Y, Zhao W, Zeng Y, Wang C. Photocatalytic CO_2 reduction over $SrTiO_3$: correlation between surface structure and activity. *Appl Surf Sci*. 2018;447:627-635.
118. Shao K, Wang Y, Iqbal M, et al. Modification of Ag nanoparticles on the surface of $SrTiO_3$ particles and resultant influence on photoreduction of CO_2. *Appl Surf Sci*. 2018;434:717-724.
119. Gholamrezaei S, Salavati-Niasari M. An efficient dye sensitized solar cells based on $SrTiO_3$ nanoparticles prepared from a new amine-modified sol-gel route. *J Mol Liq*. 2017;243:227-235.
120. Banik A, Ansari MS, Alam S, Qureshi M. Thermodynamic barrier and light scattering effects of nanocube assembled $SrTiO_3$ in enhancing the photovoltaic properties of zinc oxide based dye sensitized solar cells. *J Phys Chem C*. 2018;122(29):16550-16560.
121. Okamoto Y, Suzuki Y. Double-layer dye-sensitized solar cells using $SrTiO_3$ and $BaTiO_3$ second layer with enhanced photovoltaic performance. *J Cerma Soc Jpn*. 2015;123(1442):967-971.
122. Call RW, Alibabaei L, Dillon RJ, et al. Growth and post-deposition treatments of $SrTiO_3$ films for dye-sensitized photoelectrosynthesis cell applications. *ACS Appl Mater Interfaces*. 2016;8(19):12282-12290.
123. Burnside S, Moser JE, Brooks K, Grätzel M, Cahen D. Nanocrystalline mesoporous strontium titanate as photoelectrode material for photosensitized solar devices: increasing photovoltage through flatband potential engineering. *J Phys Chem B*. 1999;103(43):9328-9332.
124. Dom R, Chary AS, Subasri R, Hebalkar NY, Borse PH. Solar hydrogen generation from spinel $ZnFe_2O_4$ photocatalyst: effect of synthesis methods. *Int J Energy Res*. 2015;39(10):1378-1390.
125. Pan T-C, Wang SH, Lai YS, Jehng JM, Huang SJ. Study of the silver modified TiO_2 nanotube array applied to hydrogen evolution. *Appl Surf Sci*. 2014;296:189-194.
126. Jiao Z, Chen T, Xiong J, et al. Visible-light-driven photoelectrochemical and photocatalytic performances of Cr-doped SrTiO 3/TiO 2 heterostructured nanotube arrays. *Sci Rep*. 2013;3(1):2720.
127. Li M, Liu H, Song Y, Gao J. Design and constructing of mutually independent crystal facet exposed TiO_2 homojunction and improving synergistic effects for photoelectrochemical hydrogen generation and pollutant degradation. *Int J Energy Res*. 2018;42(15):4625-4641.
128. Yuan R, Ramjaun SN, Wang Z, Liu J. Effects of chloride ion on degradation of Acid Orange 7 by sulfate radical-based advanced oxidation process: implications for formation of chlorinated aromatic compounds. *J Hazard Mater*. 2011;196:173-179.
129. Harraz FA, Ismail AA, al-Sayari SA, al-Hajry A. Novel α-Fe_2O_3/polypyrrole nanocomposite with enhanced photocatalytic performance. *J Photochem Photobiol A Chem*. 2015;299:18-24.
130. Zhang Q-Q, Ying GG, Pan CG, Liu YS, Zhao JL. Comprehensive evaluation of antibiotics emission and fate in the river basins of China: source analysis, multimedia modeling, and linkage to bacterial resistance. *Environ Sci Technol*. 2015;49(11):6772-6782.
131. Reardon S. Antibiotic resistance sweeping developing world: bacteria are increasingly dodging extermination as drug availability outpaces regulation. *Nature*. 2014;509(7499):141-143.
132. Epold I, Trapido M, Dulova N. Degradation of levofloxacin in aqueous solutions by Fenton, ferrous ion-activated persulfate and combined Fenton/persulfate systems. *Chem Eng J*. 2015;279:452-462.
133. Ouyang S, Tong H, Umezawa N, et al. Surface-alkalinization-induced enhancement of photocatalytic H_2 evolution over $SrTiO_3$-based photocatalysts. *J Am Chem Soc*. 2012;134(4):1974-1977.
134. Bandara J, Weerasinghe H. Enhancement of photovoltage of dye-sensitized solid-state solar cells by introducing high-band-gap oxide layers. *Sol Energy Mater Sol Cells*. 2005;88(4):341-350.
135. Prabavathy N, Shalini S, Balasundaraprabhu R, Velauthapillai D, Prasanna S, Muthukumarasamy N. Enhancement in the photostability of natural dyes for dye-sensitized solar cell (DSSC) applications: a review. *Int J Energy Res*. 2017;41(10):1372-1396.
136. Alibabaei L, Luo H, House RL, Hoertz PG, Lopez R, Meyer TJ. Applications of metal oxide materials in dye sensitized photoelectrosynthesis cells for making solar fuels: let the molecules do the work. *J Mater Chem A*. 2013;1(13):4133-4145.
137. Selvaraj P, Roy A, Ullah H, et al. Soft-template synthesis of high surface area mesoporous titanium dioxide for dye-sensitized solar cells. *Int J Energy Res*. 2019;43(1):523-534.
138. Yahya M, Ismail M. Catalytic effect of $SrTiO_3$ on the hydrogen storage behaviour of MgH_2. *J Energy Chem*. 2019;28:46-53.

139. Yahya M, Ismail M. Synergistic catalytic effect of $SrTiO_3$ and Ni on the hydrogen storage properties of MgH_2. *Int J Hydrogen Energy*. 2018;43(12):6244-6255.

140. Yahya MS, Lew WB, Halim Yap FA, Ismail M. The catalytic effect of an inert additive ($SrTiO_3$) on the hydrogen storage properties of $4MgH_2Na_3AlH_6$. *Int J Hydrogen Energy*. 2018;43(45):20801-20810.

141. Pourmohamadian H, Rahimi-Nasrabadi M, Sheikhzadeh GA, Tabrizi HB. Preparation of $SrTiO_3$-microencapsulated palmitic acid by means of a sol–gel approach as thermal energy storage materials. *J Mater Sci Mater Electron*. 2018;29(1):794-800.

142. Diao C, Liu H, Lou G, et al. Structure and electric properties of sandwich-structured $SrTiO_3/BiFeO_3$ thin films for energy storage applications. *J Alloys Compd*. 2019;781:378-384.

143. Wang Z, Cao M, Yao Z, et al. Dielectric relaxation behavior and energy storage properties in $SrTiO_3$ ceramics with trace amounts of ZrO_2 additives. *Ceram Int*. 2014;40(9):14127-14132.

144. Wang Z, Cao M, Yao Z, et al. Effects of Sr/Ti ratio on the microstructure and energy storage properties of nonstoichiometric $SrTiO_3$ ceramics. *Ceram Int*. 2014;40(1):929-933.

145. Shi P, Zhu L, Gao W, et al. Large energy storage properties of lead-free (1-x)(0.72 Bi0. 5Na0. $5TiO_3$-0.28 $SrTiO_3$)-x$BiAlO_3$ ceramics at broad temperature range. *J Alloys Compd*. 2019;784:788-793.

146. Hou C, Huang W, Zhao W, Zhang D, Yin Y, Li X. Ultrahigh energy density in $SrTiO_3$ film capacitors. *ACS Appl Mater Interfaces*. 2017;9(24):20484-20490.

147. Yan F, Yang H, Lin Y, Wang T. Dielectric and ferroelectric properties of $SrTiO_3$–Bi0. 5Na0. $5TiO_3$–BaAl0. 5Nb0. $5O_3$ lead-free ceramics for high-energy-storage applications. *Inorg Chem*. 2017;56(21):13510-13516.

148. Gao W, Yao M, Yao X. Achieving ultrahigh breakdown strength and energy storage performance through periodic interface modification in $SrTiO_3$ thin film. *ACS Appl Mater Interfaces*. 2018;10(34):28745-28753.

149. Xie J, Hao H, Liu H, et al. Dielectric relaxation behavior and energy storage properties of Sn modified $SrTiO_3$ based ceramics. *Ceram Int*. 2016;42(11):12796-12801.

150. Cheng H, Chen Y, Sun W, et al. The enhanced dehydrogenation performances of $17MgH_2$-12Al composite with additive TiH_2. *J Alloys Compd*. 2017;704:769-775.

151. Malka IE, Pisarek M, Czujko T, Bystrzycki J. A study of the ZrF_4, NbF_5, TaF_5, and $TiCl_3$ influences on the MgH_2 sorption properties. *Int J Hydrogen Energy*. 2011;36(20):12909-12917.

152. Yao Z, Song Z, Hao H, et al. Homogeneous/inhomogeneous-structured dielectrics and their energy-storage performances. *Adv Mater*. 2017;29(20):1601727.

153. Palneedi H, Peddigari M, Hwang GT, Jeong DY, Ryu J. High-performance dielectric ceramic films for energy storage capacitors: progress and outlook. *Adv Funct Mater*. 2018;28(42):1803665.

154. Zhang GF, Liu H, Yao Z, Cao M, Hao H. Effects of Ca doping on the energy storage properties of (Sr, Ca) TiO 3 paraelectric ceramics. *J Mater Sci Mater Electron*. 2015;26(5):2726-2732.

155. Burn I, Smyth D. Energy storage in ceramic dielectrics. *J Mater Sci*. 1972;7(3):339-343.

156. Young A, Hilmas G, Zhang SC, Schwartz RW. Effect of liquid-phase sintering on the breakdown strength of barium titanate. *J Am Ceram Soc*. 2007;90(5):1504-1510.

157. Tkach A, Vilarinho PM, Senos AMR, Kholkin AL. Effect of nonstoichiometry on the microstructure and dielectric properties of strontium titanate ceramics. *J Eur Ceram Soc*. 2005;25(12):2769-2772.

158. Fergus JW. Perovskite oxides for semiconductor-based gas sensors. *Sens Actuators B*. 2007;123(2):1169-1179.

159. Chan NY, Zhao M, Huang JX, et al. Highly sensitive gas sensor by the $LaAlO_3/SrTiO_3$ heterostructure with Pd nanoparticle surface modulation. *Adv Mater*. 2014;26(34):5962-5968.

160. Trabelsi H, Bejar M, Dhahri E, et al. Raman, EPR and ethanol sensing properties of oxygen-Vacancies $SrTiO_3$-δ compounds. *Appl Surf Sci*. 2017;426:386-390.

161. Hodak SK, Supasai T, Wisitsoraat A, Hodak JH. Design of low cost gas sensor based on $SrTiO_3$ and $BaTiO_3$ films. *J Nanosci Nanotechnol*. 2010;10(11):7236-7238.

162. Karthika A, Selvarajan S, Karuppasamy P, Suganthi A, Rajarajan M. A novel highly efficient and accurate electrochemical detection of poisonous inorganic Arsenic (III) ions in water and human blood serum samples based on $SrTiO_3$/β-cyclodextrin composite. *J Phys Chem Solid*. 2018.

163. Ahmad K, Mohammad A, Mathur P, Mobin SM. Preparation of $SrTiO_3$ perovskite decorated rGO and electrochemical detection of nitroaromatics. *Electrochim Acta*. 2016;215:435-446.

164. Zhang M, Wei S, Ren W, Wu R. Development of high sensitivity humidity sensor based on gray $TiO_2/SrTiO_3$ composite. *Sens*. 2017;17(6):1310.

165. Cheng P, Wang L, Pan Y, et al. Fiber Bragg grating temperature sensor of cladding with $SrTiO_3$ thin film by pulsed laser deposition. *Laser Phys*. 2019;29(2):025107.

166. Dhiman A et al. Strontium titanate composites for microwave-based stress sensing. *JOM*. 2018;1-5.

167. Xue J, Sharma A, Shashurin A, Tomar V. A single-interface photoelectrochemical sensor based on branched TiO_2 nanorods@ strontium titanate for two biomarkers detection. *J Mater Chem B*. 2018.

168. Cazorla C, Stengel M. First-principles modeling of Pt/LaAlO 3/SrTiO 3 capacitors under an external bias potential. *Phys Rev B*. 2012;85(7):075426.

169. Liang H, Cheng L, Zhai X, et al. Giant photovoltaic effects driven by residual polar field within unit-cell-scale LaAlO 3 films on SrTiO 3. *Sci Rep*. 2013;3(1):1975.

170. Marina OA, Canfield NL, Stevenson JW. Thermal, electrical, and electrocatalytical properties of lanthanum-doped strontium titanate. *Solid State Ion*. 2002;149(1-2):21-28.

171. Moos R, Hardtl KH. Defect chemistry of donor-doped and undoped strontium titanate ceramics between 1000° and 1400°C. *J Am Ceram Soc*. 1997;80(10):2549-2562.

172. Zhang G, Jiang W, Hua S, Zhao H, Zhang L, Sun Z. Constructing bulk defective perovskite SrTiO 3 nanocubes for high performance photocatalysts. *Nanoscale*. 2016;8(38):16963-16968.

173. Wang J. *Electrochemical Sensing of Explosives, in Counterterrorist Detection Techniques of Explosives*. Amsterdam, London: Elsevier; 2007:91-107.
174. O'Mahony AM, Wang J. Nanomaterial-based electrochemical detection of explosives: a review of recent developments. *Anal Methods*. 2013;5(17):4296-4309.
175. Caygill JS, Davis F, Higson SP. Current trends in explosive detection techniques. *Talanta*. 2012;88:14-29.
176. Chen D, Zhang H, Liu Y, Li J. Graphene and its derivatives for the development of solar cells, photoelectrochemical, and photocatalytic applications. *Energ Environ Sci*. 2013;6(5):1362-1387.
177. Gao N, Fang X. Synthesis and development of graphene–inorganic semiconductor nanocomposites. *Chem Rev*. 2015;115(16):8294-8343.
178. Kim H-K, Park SH, Yoon SB, et al. In situ synthesis of three-dimensional self-assembled metal oxide–reduced graphene oxide architecture. *Chem Mater*. 2014;26(16):4838-4843.
179. Dincer I. Environmental and sustainability aspects of hydrogen and fuel cell systems. *Int J Energy Res*. 2007;31(1):29-55.
180. Singhal SC, Kendall K. *High-Temperature Solid Oxide Fuel Cells: Fundamentals, Design and Applications*. Elsevier; 2003.
181. Stathis G, Simwonis D, Tietz F, Moropoulou A, Naoumides A. Oxidation and resulting mechanical properties of Ni/8Y 2 O 3-stabilized zirconia anode substrate for solid-oxide fuel cells. *J Mater Res*. 2002;17(5):951-958.
182. Klemensø T, Chung C, Larsen PH, Mogensen M. The mechanism behind redox instability of anodes in high-temperature SOFCs. *J Electrochem Soc*. 2005;152(11):A2186-A2192.
183. Waldbillig D, Wood A, Ivey DG. Thermal analysis of the cyclic reduction and oxidation behaviour of SOFC anodes. *Solid State Ion*. 2005;176(9-10):847-859.
184. Malzbender J, Wessel E, Steinbrech RW. Reduction and re-oxidation of anodes for solid oxide fuel cells. *Solid State Ion*. 2005;176(29-30):2201-2203.
185. Shen X, Sasaki K. Highly redox-resistant solid oxide fuel cell anode materials based on La-doped $SrTiO_3$ by catalyst impregnation strategy. *J Power Sources*. 2016;320:180-187.
186. Park BH, Choi GM. Effect of anode firing on the performance of lanthanum and nickel co-doped $SrTiO_3$ (La0. 2Sr0. 8Ti0. 9Ni0. 1O3− δ) anode of solid oxide fuel cell. *J Power Sources*. 2015;293:684-691.
187. Singh S, Singh P, Viviani M, Presto S. Dy doped $SrTiO_3$: a promising anodic material in solid oxide fuel cells. *Int J Hydrogen Energy*. 2018;43(41):19242-19249.
188. Chen G, Zhu B, Deng H, et al. Advanced fuel cell based on perovskite La–$SrTiO_3$ semiconductor as the electrolyte with superoxide-ion conduction. *ACS Appl Mater Interfaces*. 2018;10(39):33179-33186.
189. Luo D, Xiao W, Lin F, Luo C, Li X. Effects of A-site deficiency on the electrical conductivity and stability of (La, Co) co-doped $SrTiO_3$ anode materials for intermediate temperature solid oxide fuel cells. *Adv Powder Technol*. Amsterdam, Netherlands Japan, 2016;27(2):481-485.
190. Shen X, Sasaki K. Robust SOFC anode materials with La-doped $SrTiO_3$ backbone structure. *Int J Hydrogen Energy*. 2016;41(38):17044-17052.
191. Macías J, Yaremchenko AA, Rodríguez-Castellón E, Starykevich M, Frade JR. Compromising between phase stability and electrical performance: $SrVO_3$–$SrTiO_3$ solid solutions as solid oxide fuel cell anode components. *ChemSusChem*. 2018.
192. Dayaghi AM, Kim KJ, Kim SJ, Sung YS, Choi GM. Oxidation of porous stainless-steel coated with donor-doped $SrTiO_3$ in anodic atmosphere of solid oxide fuel cell. *J Power Sources*. 2017;360:488-494.
193. Jo S, Yang J, Park J-Y. Electrochemcial performances of La-doped $SrTiO_3$ anode materials for intermediate temperature-solid oxide fuel cells. *ECS Trans*. 2017;78(1):1237-1243.
194. Silva ER, Curi M, Furtado JG, et al. The effect of calcination atmosphere on structural properties of Y-doped $SrTiO_3$ perovskite anode for SOFC prepared by solid-state reaction. *Ceramics International*. 2019.
195. Liu J, Wang CL, Peng H, et al. Thermoelectric properties of Dy-doped $SrTiO_3$ ceramics. *J Electron Mater*. 2012;41(11):3073-3076.
196. Johnson DC, Prieto AL. Use of strontium titanate ($SrTiO_3$) as an anode material for lithium-ion batteries. *J Power Sources*. 2011;196(18):7736-7741.
197. Enterkin JA, Setthapun W, Elam JW, et al. Propane oxidation over Pt/$SrTiO_3$ nanocuboids. *ACS Catal*. 2011;1(6):629-635.
198. Liu Y, Baumann S, Schulze-Küppers F, Mueller DN, Guillon O. Co and Fe co-doping influence on functional properties of $SrTiO_3$ for use as oxygen transport membranes. *J Eur Ceram Soc*. 2018;38(15):5058-5066.
199. Khutia M, Joshi GM, Thomas P. Dielectric relaxation of nano perovskite $SrTiO_3$ reinforced polyester resin/styrene blend for electronic applications. *J Mater Sci Mater Electron*. 2016;27(7):7685-7692.
200. Chen Y-H, Chen Y-D. Kinetic study of Cu (II) adsorption on nanosized $BaTiO_3$ and $SrTiO_3$ photocatalysts. *J Hazard Mater*. 2011;185(1):168-173.
201. Shahabuddin S, Sarih N, Afzal Kamboh M, Rashidi Nodeh H, Mohamad S. Synthesis of polyaniline-coated graphene oxide@ $SrTiO_3$ nanocube nanocomposites for enhanced removal of carcinogenic dyes from aqueous solution. *Polymers*. 2016;8(9):305.
202. Yamaguchi Y, Usuki S, Kanai Y, et al. Selective inactivation of bacteriophage in the presence of bacteria by use of ground Rh-doped $SrTiO_3$ photocatalyst and visible light. *ACS Appl Mater Interfaces*. 2017;9(37):31393-31400.
203. Wang Y, Zhang D, Wen C, Li Y. Processing and characterization of $SrTiO_3$–TiO_2 nanoparticle–nanotube heterostructures on titanium for biomedical applications. *ACS Appl Mater Interfaces*. 2015;7(29):16018-16026.
204. Yao L, Pan Z, Zhai J, Zhang G, Liu Z, Liu Y. High-energy-density with polymer nanocomposites containing of $SrTiO_3$ nanofibers for capacitor application. *Compos A: Appl Sci Manuf*. 2018;109:48-54.
205. Wu S, Ren L, Qing J, et al. Bipolar resistance switching in transparent ITO/$LaAlO_3$/$SrTiO_3$ memristors. *ACS Appl Mater Interfaces*. 2014;6(11):8575-8579.
206. Muenstermann R, Menke T, Dittmann R, Waser R. Coexistence of filamentary and homogeneous resistive switching in

Fe-doped $SrTiO_3$ thin-film memristive devices. *Adv Mater*. 2010;22(43):4819-4822.

207. Nili H, Walia S, Balendhran S, Strukov DB, Bhaskaran M, Sriram S. Nanoscale resistive switching in amorphous perovskite oxide (a-$SrTiO_3$) memristors. *Adv Funct Mater*. 2014;24(43):6741-6750.
208. Thomas D, Janardhanan C, Sebastian MT. Mechanically flexible butyl rubber–$SrTiO_3$ composite dielectrics for microwave applications. *Int J Appl Ceram Technol*. 2011;8(5):1099-1107.
209. Chen Y, Gao A, Bai L, et al. Antibacterial, osteogenic, and angiogenic activities of $SrTiO_3$ nanotubes embedded with Ag_2O nanoparticles. *Mater Sci Eng C*. 2017;75:1049-1058.
210. Okunaka S, Tokudome H, Abe R. Structure-controlled porous films of nanoparticulate Rh-doped SrTiO 3 photocatalyst toward efficient H 2 evolution under visible light irradiation. *Cat Sci Technol*. 2016;6(1):254-260.
211. Miseki Y, Fujiyoshi S, Gunji T, Sayama K. Photocatalytic Z-scheme water splitting for independent H_2/O_2 production via a stepwise operation employing a vanadate redox mediator under visible light. *J Phys Chem C*. 2017;121(18):9691-9697.
212. Alifanti M, Kirchnerova J, Delmon B, Klvana D. Methane and propane combustion over lanthanum transition-metal perovskites: role of oxygen mobility. *Appl Catal Gen*. 2004;262(2):167-176.
213. Boreave A, Tan H, Roche V, Vernoux P, Deloume JP. Oxygen mobility in lanthanum nickelate catalysts for deep oxidation of propane. *Solid State Ion*. 2008;179(21-26):1071-1075.
214. Phoon BL, Lai CW, Juan JC, Show PL, Pan GT. Recent developments of strontium titanate for photocatalytic water splitting application. *Int J Hydrogen Energy*. 2019. https://doi.org/10.1016/j.ijhydene.2019.01.166

How to cite this article: Phoon BL, Lai CW, Juan JC, Show P-L, Chen W-H. A review of synthesis and morphology of $SrTiO_3$ for energy and other applications. *Int J Energy Res*. 2019;1–24. https://doi.org/10.1002/er.4505